A METHOD FOR THE GEOGRAPHICAL INTERPOLATION OF WIND SPEED OVER HETEROGENEOUS TERRAIN

J. W. Verkaik [1]

December 11, 2001

[1]Royal Netherlands Meteorological Institute (KNMI), PO Box 201, 3730 AE De Bilt, the Netherlands. Phone: +31 30 2206 864. Fax: +31 30 2204 614. Internet : http://www.knmi.nl/samenw/hydra. e-mail: job.verkaik@knmi.nl

Contents

List of Figures

List of Tables

Abstract

A two-layer model of the atmospheric boundary layer has been used to estimate the wind speed at several locations in the Netherlands from measurements of wind speed at other locations. The model comprises a surface layer of fixed depth and an Ekman layer. Non-neutral atmospheric stability is ignored, the model is neutral. The roughness lengths for the two layers are different. They are determined from high resolution land use maps using a simplified footprint model and are therefore wind direction dependent. The model will be used to generate wind fields over inland water bodies and coastal regions. This model is preferred above internal boundary models because it handles highly heterogenous regions in a better way, and because it yields wind fields in stead of wind profiles on a line.

The estimated wind speed is compared to measurements. The test data set comprises five years of hourly averages of surface wind speed. The simulation error is assessed as functions of wind speed, wind direction, and atmospheric stability for several locations.

The tests show that the model is well suited for its purpose. The accuracy of the simulated wind speed and direction differs from station to station and depends on wind direction as well. Overall the relative error in wind speed is 10–15%. The error in wind direction is 10°–20°, depending on wind speed. However, we expect the model to perform better than this after revision of the roughness maps and/or footprint approximation used in this paper.

Chapter 1

Introduction

Knowledge of the wind climate at specific locations is of vital importance for risk assessment, engineering, and wind power potential, for example. Generally this local climatology is only available at meteorological stations. In the Netherlands these stations may be at a distance of 30–40 km from the place of interest. Over large water bodies these distances may be even larger (see Fig. B.1 for a map of the Netherlands and the wind speed measuring network operating in 2001). Because of changing roughness conditions the wind climate at the place of interest will be different from that of the meteorological station and a transformation method is needed.

In the context of the KNMI HYDRA-project the hydraulic boundary conditions are assessed for safety testing of the Dutch dikes. The wind fields over the Dutch coast and inland water bodies in extreme conditions play a major role in these tests. These wind fields are assessed from the climatological wind speed records. The density of the wind speed measuring network in the Netherlands is far too low to resolve all the details of the wind field over the Netherlands. So, a method is required that gives wind speed estimates at any desired location in the Netherlands from the wind speed measured at a number of stations scattered over the country. In the present study our main interest lies in the coastal zone and in extreme events. So the model should be capable of dealing with major roughness changes. The model should be able to handle individual cases and not only average wind speeds or wind speed distributions. The model may not need to take stability into account, since in high wind speed conditions the effects of stability are assumed to be small. The spatial resolution should be a few hundreds of meters maximum. Since we aim at a local wind climatology we do not consider high resolution numerical models, that are computationally very demanding and time consuming. Here we focus at relatively simple models that require input data that are available over long periods of time (20–30 years).

The assumption generally made when translating wind speed from one to another location is that the wind speed at elevated levels is less influenced by local terrain features than the surface wind. If so, the wind at this level is better suited for interpolation than the surface wind or can even be considered horizontally uniform. Doing translations over large distances, the full depth of the planetary boundary layer (PBL) may need to be modelled. In the presence of major roughness changes, like coast lines, internal boundary layer models (IBL-models) may be needed for a proper description of the wind in the PBL (Garratt, 1990).

In any model there is a choice to make whether or not to include stability effects. Stability dependent formulations are available for the transformation of wind speed from one level to another, the IBL-height, the geostrophic wind speed and the PBL-height. The PBL-height can not be computed from surface stability parameters as the Obukhov length. It depends mainly on the history of the surface heat flux and synoptic forcing. If stability corrections are included in the model, it has to be interpolated geographically as well somehow, and this is probably more problematic than the wind speed itself.

Previous work on surface wind speed in changing terrain with application to the Netherlands was done by Wieringa (1986), Troen and Petersen (1989), Van Wijk et al. (1990), and Kudryavtsev et al. (2000), among others. Except for Wieringa (1986) all these models utilize IBL-models.

In the present study we will use a two-layer model as in Wieringa (1986, henceforth W86) with a different roughness length for each layer (Section 2). We will illustrate the way IBL-models use roughness maps and the strong simplification that is usually involved. We will show that IBL-models are not suited for application in areas with many roughness transitions, as is quite usual in natural terrain. We will show that the two-layer model mimics the IBL development very well (Sections 3 and 3.2). Modelling the wind speed after a roughness change without actually using an IBL-model was also done successfully by Bergström et al. (1988). Our focus will be on the evaluation of the surface roughness (Section 4), since the roughness plays a major role in our interpolation method. The two-layer model will be tested by comparing measured with simulated wind speed time series (Section 5). Advantages of the two-layer model above IBL-models are its simpler physics, the unlimited number of roughnesses and transitions that can be modelled. Also, the two-layer model yields wind fields in two-dimensions at a specified height, while IBL-models describe the wind speed development on a straight line as function of height. So, for the intended application the two-layer model is better suited.

The present study is done in the framework of the KNMI HYDRA-project. In this project we focus on extreme winds. This involves the application of statistical models. Previous work at KNMI in this field was done by Rijkoort (1983), Rijkoort and Wieringa (1983), and Wieringa and Rijkoort (1983). Recently an update and re-evaluation of the statistics was performed by Smits (2001a; 2001b). In a follow-up study the extreme value analysis of the geographically interpolated wind speed time series will be compared to that of the measured wind speed. We shortly touch on this subject in this paper, however, a detailed analysis will follow in a separate paper.

Chapter 2

Interpolation models

In this section we will summarize the basic features of some of the methods used in previous studies with application to the Netherlands: Wieringa (1986, henceforth W86), Troen and Petersen (1989, henceforth WASP), Van Wijk et al. (1990, henceforth COAST), and Kudryavtsev et al. (2000, henceforth K2000). W86 will be treated in more detail since this model will be tested in this study.

2.1 Wieringa's model

W86 used a two-layer model. In the lower layer, the surface layer, Monin-Obukhov theory is used (Obukhov, 1971; Businger and Yaglom, 1971, MO-theory). Using the local roughness length the wind speed at the top of the lower layer can be computed from the measured wind speed. This is done using the logarithmic wind speed profile, strictly speaking only valid in neutral and homogeneous surface layers. In that case the wind speed U as function of height z is given by (Tennekes, 1973)

$$U = \frac{u_*}{\kappa} \ln \frac{z}{z_0}, \tag{2.1}$$

where the von Kármán constant $\kappa = 0.4$ (Frenzen and Vogel, 1995), and u_* is the friction velocity, related to the momentum flux, $u_*^2 = -\overline{u'w'}$ (u' and w' are turbulent fluctuations of the horizontal and vertical wind speed, respectively). In surface layers over homogeneous terrain z_0 is well defined and u_* is constant with height.

In the second layer the geostrophic drag relations apply (Garratt, 1992, cf. chapter 3):

$$\begin{aligned} \frac{\kappa\,(U - U_{\text{macro}})}{u_*} &= \left[\ln \frac{zf}{u_*} + A \right], \\ \frac{\kappa V_{\text{macro}}}{u_*} &= -B. \end{aligned} \tag{2.2}$$

Here A en B [-] are stability dependent parameters ($A = 1.9$ and $B = 4.5$ in neutral conditions). The Coriolis parameter f [Hz] equals $2\omega \sin\phi = 1.1 \cdot 10^{-4}$ Hz at latitude 52° north, where ω is the angular velocity of the Earth's rotation and ϕ is the latitude. U_g and V_g are the components of the macrowind. U_g is parallel to the surface wind, V_g is perpendicular to U_g. With U_g in east direction, V_g points north. We will call this layer the Ekman layer although we do not use the Ekman spiral formulae. Matching the two layers at the mesolevel [Eqs. (2.1) and (2.2)] one can deduce

$$\begin{aligned} U_{\text{macro}} &= \frac{u_*}{\kappa} \left(\ln \frac{u_*}{f z_0} - A \right), \\ |V_{\text{macro}}| &= \frac{u_*}{\kappa} B. \end{aligned} \tag{2.3}$$

In neutral conditions we do not need to know the PBL-height h. It can be determined from u_* alone. The height of the PBL is given by

$$h = \frac{u_*}{f e^A}. \tag{2.4}$$

In non-neutral conditions, however, h is an important external parameter.

Transformation of the wind speed from one to another location is done by interpolating the macrowind, which is assumed to vary only smoothly over the domain. The macrowind can be computed from the surface wind in two steps. In the first step from the surface wind speed U_s measured at height z_s and Eq. (2.1), the mesowind $U_{\rm meso}$ is computed using the local roughness length ($z_{0\rm l}$)

$$\frac{U_{\rm meso}}{U_{\rm s}} = \frac{\ln z_m/z_{0\rm l}}{\ln z_s/z_{0\rm l}}. \tag{2.5}$$

The local roughness length was derived from gustiness analysis (Wieringa, 1976; Verkaik, 2000). For the mesolevel or blending height z_m Wieringa chose 60 m. He argued that within a few kilometres distance the wind speed at the blending height will be constant. So, doing translations over small distances, less than a few kilometres, only the first step of W86 needs to be considered, and within this range the mesowind is assumed to be uniform. This step is a regionalisation of meteorological surface parameters considering the surface layer only. Examples of regionalisation of more meteorological parameters in non-neutral conditions can be found in Hutjes (1996), De Rooy (1995), and De Rooy and Holtslag (1999).

In the second step the macrowind is computed from the mesowind. W86 calculated the mesoscale roughness by averaging drag coefficients at z_m on a spatial resolution of $(5\ \mathrm{km})^2$. To this $z_{0\rm m}$ he also added the orographic drag. Using the mesoscale roughness length $z_{0\rm m}$ he computed the area-averaged friction velocity $u_{*\rm m}$ from Eq. 2.1

$$u_{*\rm m} = \kappa U_{\rm meso} / \ln\left(z_m/z_{0\rm m}\right). \tag{2.6}$$

Using Eq. (2.3) the macrowind can be computed. This macrowind is often called the geostrophic wind. However, it is not always possible to relate the geostrophic wind, deduced from air pressure gradients, to the surface wind speed using a model as simple as this (Hess, 1973; Clarke and Hess, 1975; Luthardt and Hasse, 1981; Marsden, 1987).

W86 computed the average macrowind at a number of station locations in the Netherlands. Through these points he fitted a linear sloping wind field. Using this field the inverse process was used to compute the average mesowind at any location. If the local roughness length is known the average surface wind speed can be found as well.

W86 validated this method for averages only (seasonal and yearly averages) and not for individual cases. His method is strictly neutral. However, averaging night- and daytime will diminish most stability effects. W86's method does not apply IBL-models, so in coastal zones this method may not do so well.

2.2 The WASP model

For countries participating in the European Community in the 80s the wind energy resource has been assessed in Troen and Petersen (1989). During the assessment a method was developed to estimate the regional wind climate from wind speed records at one location. This method has been worked out to a computer program called WASP[1]. Nowadays WASP is merely the standard in wind power potential assessments. Although the program is very user friendly and is using sophisticated physics, its use for our purposes is limited. WASP performs all its calculations on the Weibull distribution parameters of the input wind climate. It is not possible to generate new time series. Also stability corrections and transformations to new heights are applied to the whole wind

[1] http://www.wasp.dk

speed distribution, not to individual measurements. In stead of using WASP as is, the physics and methods used in WASP can be adopted to construct a model.

WASP corrects the measured wind speed for shelter from nearby obstacles. The shelter module needs information about the geometry, porosity and location of obstacles. Next WASP evaluates whether or not there are upwind roughness changes using a roughness map. If so, WASP computes the local wind speed profile using an IBL-model. WASP corrects the wind speed for roughness changes and also computes an effective roughness length from the upstream surface roughness. The corrected wind and the effective roughness are used in the geostrophic drag law to compute the macrowind. The reverse process is used to estimate the wind at another location. To translate the wind speed in the surface layer to different heights WASP uses MO-theory. WASP includes stability in both in the geostrophic drag law and in the MO-theory, but only as first order, linear corrections. The IBL-model is neutral and is capable of handling a limited number of roughness changes.

Comparing WASP with W86 we find many similarities and, of course, a few differences. The correction for nearby obstacles and part of the correction for nearby roughness changes are expected to gives similar results as the exposure corrections as done in W86. A rigorous comparison of these two methods will be done in the near future in cooperation with partners from the wind energy community. In the philosophy of WASP there is only one station providing wind speed information and the macrowind is assumed uniform.

2.3 The COAST model

The COAST model is a surface layer model only and above this surface layer a uniform wind is assumed. In the surface layer MO-theory is used. Van Wijk et al. (1990) tested several combinations of neutral/non-neutral wind speed profiles and neutral/non-neutral IBL-models. The model was validated for the coastal IBL in onshore wind conditions only. They concluded that the full non-neutral model performed best, although a combination of a neutral IBL-model with non-neutral wind speed profiles yielded satisfactory results as well. The COAST model can handle only one roughness transition.

Although the physics of COAST can be used to construct another model, COAST itself is not suitable for direct application in this study. It is two-dimensional (height and distance) and computationally demanding.

2.4 Kudryavtsev and Makin's model

K2000 is a two-dimensional (height and distance) model that uses MO-theory in the surface layer and geostrophic drag laws above the surface layer. It includes an IBL-model and is fully non-neutral. Although K2000 was developed as an extension to the model by Kudryavtsev and Makin (1996) to handle multiple roughness transitions, the model is poor in doing so (Kudryavtsev et al., 2000). In the philosophy of K2000 there is only one station providing wind speed information. Although the physics of K2000 can be used to construct another model, K2000 itself is not suitable for direct application in this study.

Chapter 3

Internal boundary layers

In this section we will shortly discuss the development of IBLs. At first IBL-models were intended to be used in the KNMI HYDRA-project to yield wind fields over Dutch coastal zones. At present we feel that the two-layer model is a better alternative. Downwind of large roughness changes IBL-models are expected to give a better description of the development of the wind speed profile. Therefore we will compare the two-layer model to IBL-models.

3.1 IBL-development

It should be noted that the roughness change as interpreted by IBL-models is nothing more than a change in z_0. In reality, however, this z_0-change is usually accompanied by a complex change in surface elevation (water–dike–land, grass–forest). In non-neutral conditions the stability often changes as well. The simple model discussed here does not describe these very local flow disturbances at all. Here only the development of the wind at some separation, both in height and distance, from the transition is described.

IBL-models require well defined roughness transitions, one upstream value and one downstream value. In many part of the world multiple transitions occur at short fetches. Therefore, the validation of IBL-models has mainly been restricted to short fetches. Experiments with multiple IBLs are rare (Deaves, 1981). Some models indicate that the second IBL grows faster in case the surface roughness is returning to its initial value (Duijm, 1983).

As a result major simplifications are necessary when using IBL-models. For example, in WASP the number of transitions is limited. Also, per wind direction sector the roughness transitions are assumed to occur at the same distance. An example is given in Fig. B.2. Here a roughness map is plotted for the environment of a wind mast (Houtrib) which was located close to the city of Lelystad, at the border of the IJssel-lake. The upper map shows the roughness in grey-scale, dark areas are smooth, bright areas are rough, pixels of $(100\ \mathrm{m})^2$. This map has already been simplified significantly. The resolution of the original land-use map LGN3+ was $(25\ \mathrm{m})^2$. In LGN3+ many roughness classes were present in this area, while in this map the number of roughness classes is reduced to 10. It is clear from this map that in any direction there are a large number of transitions, and that the sequence and distance of these transitions is unique for every direction. In the lower map of Fig. B.2 the roughness analysis as performed by WASP is shown. The extreme simplification is clear. Still the IBL-model needs to model the multiple roughness transitions, an application for which there has been hardly any validation. Next we will discuss the IBL-development after a 'model roughness change'.

After a change in surface roughness the momentum flux, wind speed and wind direction will adjust so that a new equilibrium state is established. Since the perturbation of the profile originates from changes at the surface, internal boundary layers will develop from the surface. Very close to the surface a new equilibrium boundary layer (EBL) will develop. Higher up in the surface layer the flow will remain undisturbed, except for a minor streamline displacement (see Fig. B.3).

Although there is some confusion about this in early papers on IBL-theory, the momentum flux is found to adjust fastest to the new surface, followed by wind speed, at last also the wind direction will adjust itself. Taylor (1987) argues that after $\sim$ 10 km homogeneous fetch surface friction velocity should be within 5% of its equilibrium downstream value. Adjustment of the wind direction takes place only after $\sim$ 100 km homogeneous fetch (Jensen, 1978).

A simple and often encountered concept is illustrated in Fig. B.4. The PBL comprises two layers, one still adapted to the upstream, and a second, close to the surface, fully adapted to the downstream terrain. Equilibrium profiles for both terrains are linked together at the IBL-height, which is given by some empirical formula. As no transition layer is included, there is a discontinuity in stress at the IBL-height δ (Elliott, 1958; Jensen, 1978).

The growth of the IBL has been described in terms of turbulent diffusion. When a passive scalar is emitted from a location on the surface it will be transported by turbulent motions in the surface layer in downwind direction and it will be lifted from the surface as well. The mean vertical displacement as function downwind distance is a measure for the growth rate of IBL's. This approach has been extended to momentum (Pasquill, 1972). Walmsley (1989) tested several formulae for the IBL-height with data and found that Panofsky and Dutton's (1984) formula fitted best:

$$\frac{\delta}{x} = B\kappa \Big/ \left(\ln \frac{\delta}{z_0} - 1 \right). \tag{3.1}$$

Here $B = \sigma_w / u_* \simeq 1.3$, according to Panofsky and Dutton. For z_0 they used the roughness length after the transition, but others argue that it should be a combination of the roughness length before and after the transition, or a the largest of both (Jackson, 1976).

For the smooth-to-rough transition the IBL grows faster than for the rough-to-smooth transition. For the IBL, the height-to-fetch ratio approximates 1/10 for both cases (Shir, 1972; Deaves, 1981). Usually the IBL-height for momentum flux equals twice that for wind speed. The EBL-height is about one tenth of the IBL-height. So the height-to-fetch ratio for the EBL, approximates 1/100.

3.2 IBL-growth in the two-layer model

The two-layer model does not include an IBL-model. However, after a roughness transition the local- and the mesoscale roughness used will be different as a result of the different length scales of their footprint. This way the typical IBL wind speed profile as in Fig. B.4 is reproduced by the two-layer model. However, the knee in the profile is fixed at the mesolevel, while the roughness lengths associated with the two parts of the profile are constantly changing with fetch. In the simple IBL-model of Fig. B.4 the knee in the profile, the IBL-height, climbs with fetch, while the roughness length remains constant.

Now we will compare the development of the 10-m wind from the two-layer model with that of IBL-models. We consider the sea–land transition where the land roughness length is 0.1 m. We use the models W86, K2000, WASP, COAST, and a surface layer model by Townsend (1965). For W86 and Townsend's model the roughness length of the sea is fixed at 0.001 m, the other models compute the drag of the sea from the wind speed. K2000 and COAST are used in near-neutral mode, the other models are neutral by themselves. The wind at 10 m over sea is fixed at 10 m s^{-1}. The results are plotted in Fig. B.8. The upper figure shows the sea–land transition, the lower figure the land–sea transition where the wind speed over land is fixed at 7 m s^{-1}. COAST is developed for onshore flow only.

Apart from Townsend's model, all models show a similar adjustment of the 10-m wind to the new surface roughness. The rate of adjustment, both at short and long fetches, in the two-layer model depends on the length scales chosen for the local- and mesoscale roughness and the mesolevel. In fact, the non-neutral version of K2000 with unstable flow over sea and stable flow over land corresponds even better to the two-layer model. It would be possible to tune the footprint length scales for closer correspondence to one of the IBL-models, but we feel that this would not lead to significant improvement of the model. So we conclude that using the two-layer model with

different footprint length scales (600 m and 3 km) for the local- and mesoscale roughness length will not lead to large errors in the surface wind speed downwind of major roughness transitions.

Chapter 4

The roughness map

4.1 Spatial data on land-use

The surface roughness is assessed from a land-use map of the Alterra[1] (LGN3+, De Wit et al. (1999)). This is a raster file covering the whole of the Netherlands with a resolution of 25 m. To each pixel a land-use class is assigned. A number of 40 classes are used in LGN3+. We assigned a roughness length to each class. In table A.1 the land-use classes and the assigned roughness lengths are listed. Outside the Netherlands a uniform roughness of 0.24 m is adopted. Two classes were added to LGN3+: runways and parking lots. This was done because in LGN3+ the concrete runways were added to the class built-up area, resulting in erroneous and way too high roughness values in airport areas, especially close to many anemometer locations. The runways were identified by hand and added to the new class with low roughness. The same applies to large parking lots in the Amsterdam Airport Schiphol area.

4.2 Surface elevation

Surface elevation is assessed from the GTOPO30[2] database. In this database the surface elevation is given at a resolution of $(1/120)^\circ$ ($\approx$ 1 km). This grid has been interpolated using spline and exported into new grid on a 500-m resolution in local (X, Y)-coordinates. Height differences are assessed by comparing the height at point (X, Y) with the neighbouring points on the 500-m grid.

The roughness length due to orography $z_{0\mathrm{H}}$ is computed from

$$z_{0\mathrm{H}} = 0.2 \cdot \Delta H^2 / L, \tag{4.1}$$

where ΔH is the height difference over distance L (Agterberg and Wieringa, 1989).

The resolution of GTOPO30 is not enough to resolve small hills, dikes, etc. In the coming years a high-resolution elevation map of the Netherlands will become available. Then this part of the roughness map asks for revision.

It should also be noted that although orography adds to the roughness on large scales, on small scales orography may induce acceleration of wind and complex circulation patterns around hills (Jackson and Hunt, 1975; Jacobs, 1984). In the two-layer model these effects are not incorporated. This may lead to very local errors in the wind field in the vicinity of dikes and hills. So measurements from locations where these phenomena can be expected need to be interpreted with care.

[1] http://cgi.girs.wageningen-ur.nl/cgi/projects/lgn/index_nl.htm
[2] http://edcdaac.usgs.gov/gtopo30/gtopo30.html

4.3 Area-averaged surface roughness

A suitable manner to aggregate surface roughness is to model the drag coefficients at the blending height (Claussen, 1990). This method was also used by Wieringa (1986). This method gives stronger weight to the larger roughnesses in the averaging domain.

The drag coefficient is defined as $C_d \equiv (u_*/U)^2$ and using Eq. (2.1) it can be expressed as

$$C_d = \left[\frac{\kappa}{\ln(z/z_0)}\right]^2. \tag{4.2}$$

The roughness due to orography can also be expressed as a drag coefficient by this equation and this drag can be added to the 'skin drag'. Eq. (4.2) can be inverted the compute the roughness length from the total drag.

4.4 Footprint approximation

The footprint is the surface area contributing to the flux or concentration of an atmospheric entity at a certain point. The footprint depends on the entity under consideration, the atmospheric stability and of measuring height (Schmid, 1994; Horst and Weil, 1992; Horst, 1999). In Fig. B.5 an example is given. The terrain here consists of water on the east and land on the west. At some distance inland we imagine a measuring tower with sensors at two heights. The wind is onshore. The footprint of the lower sensor is small and is close to the tower. This is indicated by the ellipsoids at the surface, partially over land and partially over water. The inner ellipsoid could represent the area which determines 50% of the measured entity by this sensor, the outer ellipsoid represents 90% area. All numbers and scale ratios in this example are fictitious.

However, here we will make a simple approximation to the footprint using the following procedure. The area surrounding the evaluation point is split into 72 sectors 5° wide. For each pixel i in sector j the drag coefficient at the blending height is determined from the equation

$$C_{d,i} = \left[\frac{\kappa}{\ln(z_{bh}/z_0)}\right]^2. \tag{4.3}$$

The roughness length is determined from Table A.1. The drag coefficient of water is wind speed dependent and will not be added to the total drag at this stage.

A weighted average of $C_{d,i}$ is computed using the weight function

$$W(x_i, D) = \exp(x_i/D), \tag{4.4}$$

where x is the distance from the source area to evaluation point. So the average drag of sector j coefficient given by

$$C'_{d,j} = \frac{\sum_i W(x_i, D) \cdot C_{d,i}}{\sum_i W(x_i, D)} \tag{4.5}$$

Also the fraction the surface covered ($f'_{w,j}$) by water is determined. Only the source area up to a distance of $3 \times L$ is considered.

Now the direction dependent $C'_{d,j}$ and $f'_{w,j}$ are smoothed using a weighted moving average:

$$C_{d,j} = \sum_{k=-2}^{k=2} w_k \cdot C'_{d,j+k} \quad \text{and} \tag{4.6}$$

$$f_{w,j} = \sum_{k=-2}^{k=2} w_k \cdot f'_{w,j+k}, \tag{4.7}$$

where $w_{-2,-1,..+2} = \{0.08, 0.13, 0.18, 0.22, 0.18, 0.13, 0.08\}$ (see Fig. B.6).

4.5 Drag relation for water

The total drag at the evaluation point for wind directions in sector j is computed from

$$C_d = C_{d,j} + f_{w,j} \cdot C_{water}\,(U)\,, \tag{4.8}$$

where the drag of water can be expressed using Eq. (4.2) and the Charnock relation

$$z_0 = \alpha \cdot u_*^2/g, \tag{4.9}$$

where g is the acceleration of gravity [9.82 m s^{-1}] and for α the value 0.017 is used, which applies to the open ocean (Charnock, 1955; Garratt, 1977). For shallow waters, however, values as large as 0.032 have been reported for α (Benschop, 1996). Basically, α is determined by the wave conditions which in turn are a function of wind speed, water depth and wave age. Often a lower limit is set to z_0: $1.5 \cdot 10^{-5}$ m. If the depth of the water limits the wave growth there may also be an upper limit.

For the wave growth and water rise the drag relation for water is crucial. However, the wind is only a weak function of this relation. The reason for this is the fact that the wind speed always depends on z_0 in a logarithmic way: $U \propto \ln(z/z_0)$. From this the following sensitivity relation can be derived:

$$\frac{dU}{U} = -\frac{1}{\ln(z/z_0)}\frac{dz_0}{z_0}. \tag{4.10}$$

With $z = 10$ m and $z_0 = 0.001$ m the first factor on the right-hand-side of Eq. 4.10 is about 0.1. This means that a 100% error in z_0 yields only a 10% error in U. In this paper we will validate the model on the wind speed, not on wave growth or water rise. Because of the weak sensitivity of U on $z_{0\text{water}}$ it will be hard to monitor errors in the choice for the drag relation for water. It is probably better to test for this when validating the wave growth and water rise directly.

Chapter 5

Validation of the two-layer model

In this chapter we will test the two-layer model in several ways. The surface wind speed and direction will be used for this purpose. The success of the model depends strongly on the roughness map. Therefore the local roughness lengths will be compared to that of gustiness analysis. Unfortunately, no direct validation of the mesoscale roughness is possible. Its quality has to be assessed indirectly from the simulated surface wind.

5.1 Comparison of gustiness and land-use derived roughness lengths

In the lower layer of the two-layer model the gustiness derived roughness length ($z_{0\mathrm{gust}}$) is used to transform the measured wind speed to the mesolevel. However, $z_{0\mathrm{gust}}$ is only available at the station locations. For the downward transformation at any other spot the roughness length has to be computed from the land-use map ($z_{0\mathrm{map}}$). Therefore, the success of the model will partially depend on the quality of the match between these two. To assess the possible mismatch $z_{0\mathrm{map}}$ and $z_{0\mathrm{gust}}$ are compared at the station locations.

The error will be expressed as follows. The ratio (f_1) of the 60-m wind to the 10-m wind is computed from Eq. (2.5) using $z_{0\mathrm{gust}}$:

$$f_1 = \ln(60/z_{0\mathrm{gust}}) / \ln(10/z_{0\mathrm{gust}}),$$

and the ratio f_2 is that of the 10-m wind to the 60-m wind using $z_{0\mathrm{map}}$:

$$f_2 = \ln(10/z_{0\mathrm{map}}) / \ln(60/z_{0\mathrm{map}}).$$

The error factor is

$$\text{Error factor} = f_1 \cdot f_2.$$

With a perfect match the error factor equals unity.

In Fig. B.7 the error factor is plotted for 34 stations. For each station $z_{0\mathrm{gust}}$ has been determined from gustiness records of the last couple of years. It has been computed for 18 wind direction sectors of 20° wide. From this figure it can be seen that for sectors with a low $z_{0\mathrm{gust}}$ the error is usually less than 10%. The cluster of points with high $z_{0\mathrm{gust}}$'s comprises most of the onshore stations. In this cluster there is a slight trend of increasing error with increasing $z_{0\mathrm{gust}}$. This implies that for large $z_{0\mathrm{gust}}$'s, the $z_{0\mathrm{map}}$'s tend to fall behind. Close examination of some notorious errors reveals that often the land-use map is in error. This is partially due to its finite resolution. With a pixel size of (25 m)^2 isolated obstacles may not be resolved. These obstacles can have a large impact on the observed gustiness and wind speed.

In the low $z_{0\text{gust}}$-sectors there is often water present in the footprint The error factor in these sectors is more often larger than 1. This could be the results of our choice for $\alpha = 0.017$ in Eq. (4.9). This value must be considered as a minimum, and may need enhancement.

On average the error factor is 102.3 with a standard deviation of 0.076. This means the mismatch between $z_{0\text{map}}$ and $z_{0\text{gust}}$ may result in an very small bias (2.3%) and average scatter of 7.6% in wind speed. The error will be smaller over open terrain since the largest errors are the result of unresolved obstacles.

5.2 Validation of surface wind speed

The most direct way to assess the quality of the two-layer model is to compare the estimated wind at station locations with the measured wind speed. In this section this will be done in three ways. First, we will investigate the average difference (bias) between the estimated and measured wind speed. Second, we will investigate the dependence of the differences on wind speed and direction for a number of stations.

5.2.1 Description of the test data set

We will use a five-year data set of hourly measurements from nearly all stations available in the Netherlands for the period 1996–2000. This set comprises about 50 stations listed in Table A.2. The wind data used in this study is 'potential' wind data. This means that the mesowind is calculated from the measured wind speed using the local surface roughness, and from this the wind speed at $z_{\text{ref}} = 10$ m over a hypothetical terrain with roughness length $z_{0\text{ref}} = 0.03$ m is computed ($z_{0\text{ref}} = 0.002$ m over water). The latter is called the potential wind speed (U_{p}). This approach has been adopted from Wieringa (1976). The local roughness length is derived from gustiness analysis, but in this study a different gustiness model has been used than Wieringa (1976) did. Here we used Beljaars's (1987) gustiness model which is more flexible in modelling various measuring chains (Verkaik, 2000).

The potential wind speed can be interpreted as a wind speed that has been stripped from very local roughness features. This makes the potential wind speed better suited for comparison with wind speed measurements from nearby stations than the measured wind speed itself. In the computation of the potential wind also changes of roughness in time are corrected for. Note that the roughness map is not time-dependent, only the last decennium digital high-resolution land use maps have become available. When simulating the wind field for historical cases, simulation errors may be induced by the implicit assumption of a constant roughness map in areas where there have actually been large roughness changes in time.

Because the potential wind speed is computed from the mesowind with a fixed roughness length, it is very easy to compute the mesowind from the potential wind speed. The mesowind is the product of U_{p} and the factor

$$U_{\text{m}}/U_{\text{p}} = \ln\left(z_{\text{m}}/z_{0\text{ref}}\right) / \ln\left(z_{\text{ref}}/z_{0\text{ref}}\right), \tag{5.1}$$

which equals 1.31 with $z_{\text{m}} = 60$ m and $z_{\text{ref}} = 10$ m over land and 1.21 over water.

The two-layer model is used in quasi-stationary mode. Using hourly averages of wind speed minimizes any effect of time delay. This delay is caused by the separation distance between the sensor and the footprint. The air needs time to pass over the footprint area before it reaches the wind speed sensor. Within one hour, however, the air traverses more than 10 km if the wind speed is over 3 m s^{-1}.

5.2.2 Interpolation of the macrowind

The interpolation of the macrowind is done in two ways. We start by simply averaging the macrowind over the whole domain, i.e. a uniform macrowind is assumed. Next we will use the

method by Barnes (Krishnamurti and Bounoua, 1996). Here the wind speed at a grid is computed from that at the measuring points by a weighted average. The weight function is given by

$$w\,(d,R) = \exp\left(-\frac{4d^2}{R^2}\right), \tag{5.2}$$

where d is the distance from the grid point to the measuring point, and R is a length scale (radius of influence). At a distance of $r = R$ the weight function has diminished to less than 0.02. The resulting field is the first guess.

Now at the measuring locations the wind speed is estimated by averaging the nearest $N_{\rm point}$ grid points using the same weight function. The difference between the estimated and input values can now be used to start the procedure again. The interpolated difference field is added to the first guess. By this iteration the grid field can be adjusted until the difference between input and estimated values has become below a certain limit, or the iteration can be stopped after $N_{\rm it}$ loops.

The tests in this report are performed using $N_{\rm point} = 4$ and $N_{\rm it} = 3$, and using R-values of 20, 70, and 140 km. Together with the uniform macrowind assumption we have four runs:

run 0	Uniform macrowind
run 1	$R = 140$ km
run 2	$R = 70$ km
run 3	$R = 20$ km

The larger R the more the wind field is smoothed. So the results with $R = 140$ km will resemble closest to that of the uniform macrowind assumption. The interpolation is performed on the eastward and northward components of the macrowind separately. The macrowind is gridded to a rectangular grid with 40 km spacing.

5.2.3 Bias in simulated wind speed

The bias of the simulated wind speed is assessed from the test data set as follows. All stations but one are used to estimate the macrowind. Next, the macrowind is interpolated to a regular grid. Using this gridded macrowind, the macrowind at the excluded station is estimated. Then this macrowind is transformed to the surface wind. This procedure is repeated for every station. The difference between simulated and measured wind speed is computed on an hourly basis. This difference and its square are averaged to yield the bias and the scatter of the simulations.

The results are plotted in Figs. B.9–B.12. Assuming a uniform macrowind leads to an underestimation of the surface wind over the North Sea and an overestimation over land (see Fig. B.9). This indicates that the estimated macrowind over land is actually lower than over sea. In Fig. B.10 ($R = 140$ km) the gradient in bias is much smaller. In Fig. B.11 ($R = 70$ km) the pattern becomes irregular, indicating that the resulting bias is not caused by the interpolation length scale. In Fig. B.12 ($R = 20$ km) the pattern exhibits stronger irregularities. Apparently some smoothing of the macrowind is required and a length scale of the order of 70 km seems to be convenient. For this run the bias averaged over all station is -0.04 m s^{-1}, standard deviation 0.51 m s^{-1}. The largest bias is found at station 254 Meetpost Noordwijk ($+1.2$ m s^{-1}).

5.2.4 Wind speed dependence of error in simulated wind speed

In the Figs. B.13, B.17, B.21, and B.25 the simulated wind speed is plotted as function of the measured wind speed for the four runs for the stations 225 IJmuiden, 240 Schiphol, 348 Cabauw, and 356 Herwijnen. Station 225 was chosen because it is a coastal station. Station 240 is of special importance to RIZA and especially at this station the simulations were poor. Stations 348 and 356 were chosen because their environment is relatively simple, which simplifies the interpretation of the simulation performance. The measured wind speed has a resolution of 1 m s^{-1} and these integer values have also been used to bin the data. Only bins with 10 or more points are plotted. For run 2 the error bars are plotted which indicate the standard deviation of the data in the bin. The error bars for the other runs are of the same magnitude.

For these stations run 0 (uniform macrowind) underestimates high wind speeds and overestimated low wind speeds. This is result of averaging the macrowind over all stations. Local extremes, both in high and low wind speed, are not reproduced since these extremes do not occur at all stations simultaneously. Decreasing R will reduce this phenomenon. Using a very small R will effectively couple the macrowind at the test station to that of the closest available input station. For all runs the lowest wind speeds are overestimated. Apart from this, the difference between estimated and measured wind speed does not depend strongly on wind speed. The standard deviation of the error slightly increases with wind speed, which means that the relative error decreases with wind speed. The differences between the runs 1, 2, and 3 are relatively small. For station 240 Schiphol all runs underestimate the wind speed.

5.2.5 Wind direction dependence of error in simulated wind speed

For the same stations as in the previous section the difference in average wind speed is plotted as function of wind direction in Figs. B.14, B.18, B.22, and B.26. Only the results for run 2 ($R = 70$ km) are given. The measured wind direction has been used to bin the data. Cases with measured wind speed smaller than 2 m s^{-1} are ignored.

It is clear that for all stations the difference between estimated and measured wind speed depends on wind direction. Fig. B.13 shows that run 2 underestimates the wind speed at station 225 IJmuiden. Fig. B.14, however, shows that this underestimation occurs only for eastern winds (offland). In north-east direction the underestimation is largest. This coincides with the IJmuiden city area in the roughness footprint. This is shown in Fig. B.15 and B.16. A land use map of the environment of this station is given (area [20 km]^2) in Fig. B.15. Fig. B.16 shows for the mesoscale and local roughness length as derived from the map. Underestimation of the wind speed may be the result of overestimation of the roughness length.

Fig. B.17 shows a strong underestimation of the wind speed for station 240 Schiphol. Fig. B.18 shows that this is mainly due to winds from southwest direction, but also in the northeast and west-northwest the wind speed is underestimated. Figs. B.19 and B.20 show that all these directions coincide with built up areas in the footprint for the mesoscale roughness. This suggests that the mesoscale roughness is overestimated in directions with built up areas.

For station 348 Cabauw run 2 overestimates the wind speed (Fig. B.21). The main overestimations are found in the directions southeast and southwest (Fig. B.22). The village Lopik in eastern direction (Fig. B.23) is well reflected in the local roughness length (Fig. B.24). In the southeast direction the mesoscale roughness footprint comprises the river bed of the Lek and the village Ameide across the river at a distance of 2–4 km. However, the mesoscale roughness is no larger than 0.1 m in this direction. The same applies to the river bed south of the village Schoonhoven and Schoonhoven itself at a distance of 8 km in southwest direction. In these cases the mesoscale roughness length may be underestimated.

Although run 2 in Fig. B.25 shows only small errors for station 356 Herwijnen, Fig. B.26 shows there is an overestimation of the wind speed around the northeast direction. The terrain nearby this location is very smooth, as is indicated by the very low local roughness (Fig. B.28). The villages in these direction are at some distance (> 3 km, Fig. B.27). The overestimation of the wind speed suggests the mesoscale roughness is underestimated.

All together it might be the case that the length scale for the mesoscale roughness footprint has been chosen too small. In this analysis a value of 3 km has been used. Increasing this length scale will lead to a smoothing over a larger area. It can cause the mesoscale roughness in rough areas like 225 IJmuiden (east) and 240 Schiphol to decrease, and in smooth areas as 348 Cabauw and 356 Herwijnen to increase. Additional runs are necessary to optimize the footprint length scale.

5.3 Error in wind direction

The error in wind direction is plotted for the stations 225 IJmuiden, 240 Schiphol, 348 Cabauw, and 356 Herwijnen in the Figs. B.29–B.32. In the upper figures the bias in wind direction is plotted (Estimated−Measured) and in the lower figure the standard deviation of the bias is plotted. In cases of low wind speed the wind direction may not be well defined and therefore the bias and standard deviation are computed for different thresholds for the wind speed. For the wind direction, the x-axis, the measured wind direction is used. For the threshold wind speed the measured wind speed is used.

From the standard deviations (b-figures) it is clear that the error in wind direction decreases with increasing wind speed, as expected. For low wind speed the standard deviation is as large as 20°, while for high wind speed it is less than 10°. Considering the rounding of the measured wind direction at tens of degrees, the wind direction error is small for these cases.

Except for station 348 Cabauw the bias in wind direction does not depend strongly on wind speed. Comparison with the Figs. B.14, B.18, B.22, B.26 reveals a strong correlation of the wind direction bias with the wind speed error. Overestimation of the wind speed goes along with a positive bias in wind direction, and vice versa. This correlation can be explained as follows.

In the surface layer there is no change in wind direction with height. Going down from the top of the Ekman layer to the top of the surface layer the wind backs, i.e. the wind direction changes from west to southwest for example. The angle of turning increases with the roughness length. So in case the mesoscale roughness length is underestimated the wind backs too little resulting in a positive bias in wind direction. Meanwhile the wind speed decreases too little resulting in an overestimation of the wind speed.

The fact that overestimation of the wind speed is accompanied by a positive bias in wind direction and vice versa indicates that it is the mesoscale roughness that is under- or overestimated, and not the local roughness.

5.4 Distribution of extremes

The simulated wind speed has been subjected to extreme value analysis. This has been done by selecting storm events and using the conditional Weibull distribution (see Smits (2001b) for details). In this analysis the measured and estimated *potential* wind speed are used. Since the simulated time series period is only five years, analysis will not be extended to the very low frequencies. Results are plotted for wind speeds with a return period of 1 year in the Fig. B.33 for season January–February.

The differences in the 1-year wind speeds for this season can be up to 3 or 4 m s^{-1}. For the 10-year wind speeds (not shown) the pattern looks familiar but the differences are just a bit larger. The largest difference is found at the offshore station 254 Meetpost Noordwijk: +4.0 m s^{-1} and +7.0 m s^{-1} for 1-year and 10-year wind speed respectively. But at onshore locations differences can be of the same magnitude, e.g. station 240 Schiphol: −3.6 m s^{-1} and −4.6 m s^{-1} respectively. The average difference over all stations is small: −0.4 m s^{-1} for the 1-year wind speed, and −0.5 m s^{-1} for the 10-year wind speed.

The geographical interpolation of wind speed is a way smoothing the wind field. Since extreme events in wind speed can be local in time and space we expect that the return levels would be reduced significantly by the interpolation. In the Figs. B.13, B.17, B.21, and B.25 this phenomenon is illustrated. At all stations run 0 (uniform macrowind) overestimates low wind speeds and underestimates high wind speeds. In the return levels the reduction also appears progressively: −0.7 m s^{-1} for the 100-year wind speed. These results, however, are not intended to be conclusive as the test data set comprises only 5 years. The integration of physical interpolation techniques for wind speed with statistical analysis of extremes lies beyond the scope of this report and will be elaborated on in the next phase of the KNMI HYDRA-project.

5.5 Influence of stability

5.5.1 Influence on the wind speed profile, IBL growth, and footprint area

The energy balance of the surface determines the stability of the surface layer. In case the surface temperature is higher than the temperature of the air close to the surface, the surface will heat the air. By this the air will expand, its density will drop, and the warm air starts to rise and will be replaced with cool air from aloft. This process increases the vertical mixing of air: convective turbulence. The boundary layer is said to be *unstable*. This situation occurs at sunny days. The PBL can be about 1 km deep. In case the difference in temperature between the surface and the air is small and/or the wind speed is high, the boundary layer is nearly-neutral. Vertical mixing of air is mainly due to mechanic turbulence, i.e. turbulence caused by surface roughness and obstacles. In case the surface is colder than the air, turbulence is depressed. The boundary layer is *stable* and there is hardly any vertical mixing of air. This typically occurs at night. The stable boundary layer is often very shallow: 50-100 m.

In unstable cases the difference between the wind speed and direction at different heights will be smaller, and in stable cases it will be larger than in the neutral case. However, stability will not only influence the wind profile. Stable stratification depresses vertical mixing and so limits the growth rate of IBLs. Associated with this is an increase in footprint area. In unstable stratification IBLs grow faster and footprints are smaller (Kljun et al., 1999).

5.5.2 Information on stability and PBL height

The physics of the two-layer model can incorporate stability completely. Practical application then requires stability parameters as well as boundary layer height information over the complete area of interest. The stability parameter used most widely, the Obukhov length, can be determined from surface observations like wind speed, cloud cover, air temperature, outgoing thermal radiation, time of day, etc. (Holtslag and Van Ulden, 1983; Beljaars et al., 1989; De Rooy and Holtslag, 1999). The necessary information is available at only 16 stations in the Netherlands (see the stations with stars in Table A.2).

The energy balance of the surface is determined by its radiation balance, thermal properties, soil type, moisture content, roughness, etc. This means that the energy balance and so the stability is also strongly related to land use. However, even an area homogeneous in land use may be inhomogeneous in moisture content as the results of irregular precipitation patterns (Mahrt, 2000).

The height of the PBL can not be determined from surface observations alone. In the Netherlands it can be deduced from radiosonde launchings four times a day at station 260 De Bilt. Shallow night-time boundary layer heights can be deduced from SODAR measurements at a few research locations and at Amsterdam Airport Schiphol (station 240).

So we see that it is extremely difficult to get the stability information really right. Without running complex high resolution models stability and boundary layer height information will not be available. Running those models can be considered for selected cases, but certainly not for long time series. Doing so is not intended in the KNMI HYDRA-project. At this stage we do not intend to run the two-layer model in non-neutral form either. We can, however, assess the simulation error as function of stability at the stations where stability parameters are available.

5.5.3 Statistics of $1/L$

For our test period 1996–2000 we computed the Obukhov length L from surface observations if possible. L is negative in unstable conditions and positive in stable conditions. In unstable cases $|L|$ represents the height where the convective production of turbulence becomes more important than the mechanical production. In neutral conditions L becomes extremely large. Therefore $1/L$ is a better parameter to base our statistics on. We will compute averages and standard deviations as an indication of its scatter, however, $1/L$ is certainly not normally distributed.

For all inland stations the average stability is stable, range 0.02–0.04 m^{-1}, except for station 275 Deelen. Here $\overline{1/L} = -0.004$ m^{-1}. For all these stations the standard deviation in $1/L$ is less than 0.14 m^{-1}. The stability parameters from station 310 Vlissingen were rejected since they are probably erroneous and dominated the statistics ($\overline{1/L} = -0.3 \pm 3.5$ m^{-1}). At the coastal station 330 Hoek van Holland the average stability is unstable, -0.02 ± 0.33 m^{-1}. The unstable stratification at the coast is caused by the sea water usually being warmer than the air above it. Averaged over all stations $\overline{1/L} = 0.025 \pm 0.087$ m^{-1}.

Next we consider the hour by hour differences between the stations and the hourly average over all stations. For station 330 Hoek van Holland $1/L$ deviates from the average over all stations. On an hourly basis this difference is -0.04 ± 0.29 m^{-1}. Excluding station 330 Hoek van Holland as well, the correlation coefficient between hourly values of $1/L$ at a station and the average over all stations is in the range 0.52–0.82. For these stations the average deviation is usually less than 0.01 m^{-1} but the standard deviation is about 0.06–0.09 m^{-1}.

So there are large stability variations over the land from place to place. The difference between the stability over land and sea is even much larger, although there is only one coastal station to verify this.

5.5.4 Sensitivity of the model to stability changes

In the present two-layer model we assume neutral stability. If the stability and PBL-height over the whole land would be the same, the neutral two-layer would still do very well. The effect of stability on the upwards transformation of the wind would for a large portion be cancelled by the downwards transformation. Note that this is only true when the wind is estimated at the same height as it is measured. So the part of the stability fluctuation that is the same over the whole land will not lead to errors in the simulated wind. It is the local variation of stability that causes stability dependent errors.

From the statistics of $1/L$ we see that there are relative small inland fluctuations in stability that appear random-like. The stability over land is stable for most of the time. At sea, however, the stability is usually unstable and the difference with the stability over land can be significant. The transition in stability at the coast is sharp, stations close to the coast behave completely like inland stations.

The warm gulf stream and the large inertia of the sea surface temperature are the main causes for the difference in stability. For the inland water in the Netherlands the situation may be a bit different. Here is no gulfstream and the water is so shallow that its temperature will respond quickly to the insolation and air temperature. This means that the inland water will behave more like a land surface and the difference in stability is smaller. However, at this moment we have no data to verify this.

Since most input stations are over land and our area of interest is over water we can expect an underestimation of the wind speed over water, as will be explained. Over land the boundary layer is stable. So the difference between the measured surface wind speed and the wind speed at higher level will be larger than in the neutral case. This higher wind speed is well mixed downward in the unstable boundary layer over the water. So in reality the wind speed over the water will be larger than we expect from the neutral model. The magnitude of the error can be assessed as follows. For now we consider the surface layer only, where the wind speed gradients are largest. We assume the following conditions: heat flux density over land -50 W m^{-2}, roughness length 0.3 m ($1/L = 0.02$ m^{-1} with $U_{10} = 3.5$ m s^{-1}); heat flux density over water $+100$ W m^{-2}, roughness length 0.001 m ($1/L = -0.03$ m^{-1} with $U_{10} = 7.5$ m s^{-1}). We transform the wind speed from 10 to 60-m height over land and then transform it downwards over water for different wind speeds. In the next table we compared the ratios of the wind speed over water to the wind speed over land. In the neutral case this ratio is 1.27.

U_{10} (m s^{-1})	Ratio	Error (%)
5	1.55	22
6	1.46	15
7	1.40	10
8	1.37	7.9
9	1.35	6.3
12	1.32	3.9
15	1.30	2.4

We see that in the non-neutral case the ratio is larger. However, the underestimation of the wind speed over water declines rapidly if the wind speed increases.

5.5.5 Experimental assessment of stability error

As the wind speed increases the boundary layer becomes neutral. So errors due to stability effects are expected to vanish in high speed conditions. There is a slight decrease in relative error in the wind speed for increasing wind speed (Figs. B.13, B.17, B.21, B.25). This error is contaminated with the error in the mesoscale roughness, however. A better indication is the scatter in wind direction. Here we see a strong decrease with increasing wind speed (Figs. B.29, B.30, B.31, B.32).

In Fig. B.34 the cumulative distribution of $1/L$ for station 240 Schiphol is plotted for different wind directions. The distribution of stability is clearly dependent on wind direction. This is the result of the relation between stability and the weather on synoptic scales. In Fig. B.35 the relative error in wind speed is plotted as function of $1/L$. All results are sorted by $1/L$ in increasing order, then 30 points are averaged and the average of the error is plotted against the average of $1/L$. This is done for different wind directions.

In the direction 240° the wind speed is strongly underestimated and this also shows up in Fig. B.35. For the other directions, however, we see an overestimation of the wind speed for stable stratification. In neutral cases the error is small, and in unstable cases the wind speed is underestimated. This is exactly what we expect. The stability at this station is on average not different from the rest of the country. However, if the local stability is stable, the high momentum wind speed from aloft is poorly mixing downwards, so the measured wind speed is smaller than the estimated wind speed, and vice versa.

Chapter 6

Conclusions and Recommendations

The two-layer model was successfully applied to simulate the surface wind speed and seems suited for its purpose within the KNMI HYDRA-project: estimation of wind speed and direction at locations where no measurements are available. The model handles areas with complex topography very well. This is the major advantage of the two-layer model over IBL-models. The two-layer model is relatively simple and fast. The required input information is also simple.

The accuracy of the simulated wind speed and direction differs from station to station and depends on wind direction as well. Overall the relative error in wind speed is 10–15%. The error in wind direction is 10°–20°, depending on wind speed. However, we expect the model to perform better than this after revision of the roughness maps and/or footprint.

The roughness map includes the roughness caused by orography. The orographic roughness map needs revision when better elevations maps of the Netherlands become available. The effect of small-scale orography likes dikes on the roughness may then be represented better. The two-layer model, however, does not model the complex, local flow patterns that can be caused by orography. It only responds to the increased roughness.

The local roughness length compares well to that derived from gustiness analysis at the measuring stations. The evolution of the wind speed after a change in surface roughness are well mimicked by the two-layer model.

Assuming a uniform macrowind field yields overestimation of the wind speed over land and an underestimation over sea. The smoothing of the macrowind using the Barnes method performs best with a length scale between 70 and 140 km. Additional runs are recommended to optimize this parameter. In relation to this the number of stations needs to be considered as a parameter as well. The comparison of simulated and measured wind speed reveals that some stations always give bad results. These stations may need to be excluded from future analysis.

The roughness map, more particularly, the mesoscale roughness needs adjustment. At this moment the roughness of urban areas is overestimated. It results in an underestimation of the wind speed and a bias in wind directions where urban areas are present in the footprint. It may be solved by choosing a different footprint length scale. Otherwise the roughness length associated with built-up areas may need revision.

The scatter in the wind speed error is about 1–2 m s^{-1}, nearly independent of wind speed. The scatter in the wind direction decreases with wind speed. For wind speeds over 2 m s^{-1} it is about 20°, but for wind speeds over 8 m s^{-1} it is usually less than 10°. So in extreme high wind speeds this error is expected to be small.

The interpolation procedure averages local extreme events of the wind speed over the whole country to some extend. As a result the return levels of the simulated wind speed averages over all stations are always smaller than that of the measured wind speed. In the next phase of the

KNMI HYDRA-project this issue needs to be addressed extensively.

The stratification over land is stable most often. Over sea, however, the stratification is most often unstable. Since most wind speed measuring points are over land, the wind speed over sea may be underestimated. This underestimation becomes small in high wind speed conditions, less than 5% for a wind speed of 10 m s^{-1} at 10-m height over land. The local stability fluctuations cause errors in the estimated wind speed. In unstable conditions the wind speed can be underestimated 20–30%. In stable conditions the error is usually smaller than 10%. These results are based on the analysis of one station only, and it is recommended to investigate more stations in this way.

Acknowledgements

The present study is a contribution of KNMI to the KNMI HYDRA-project supported for RIKZ ("Rijksinstituut voor Kust en Zee" = "National Institute for Coastal and Marine Management" and RIZA ("Rijksinstituut voor Integraal Zoetwaterbeheer en Afvalwaterbehandeling" = "Institute for Inland Water Management and Waste Water Treatment"). In the KNMI HYDRA-project the hydraulic boundary conditions are assessed for safety testing of the Dutch dikes.

This reported benefitted from useful feedback given by Hans de Waal (RIZA), Janneke Ettema, Ilja Smits and Albert Klein Tank (KNMI).

Bibliography

Agterberg, R. and Wieringa, J., 1989: Mesoscale terrain roughness mapping of the Netherlands. *Technical Report* **TR-115**. Royal Netherlands Meteorological Institute.

Beljaars, A. C. M., 1987: The influence of sampling and filtering on measured wind gusts. *J. Atmos. Oceanic Technol.* **4**, 613–626.

Beljaars, A. C. M., Holtslag, A. A. M. and Van Westrhenen, R. M., 1989: Description of a software library for the calculation of surface fluxes. *Technical Report* **TR-112**. Royal Netherlands Meteorological Institute.

Benschop, H., 1996: Windsnelheidsmetingen op zeestations en kust stations: herleiding waarden windsnelheid naar 10-meter niveau. in Dutch. *Technical Report* **TR-188**. Royal Netherlands Meteorological Institute.

Bergström, H., Johansson, P.-E. and Smedman, A.-S., 1988: A study of wind speed modification and internal boundary-layer heights in a coastal region. *Bound.-Layer Meteor.* **42**, 313–335.

Businger, J. A. and Yaglom, A. M., 1971: Introduction to Obukhov's paper 'Turbulence in an atmosphere with a non-uniform temperature'. *Bound.-Layer Meteor.* **2**, 3–6.

Charnock, H., 1955: Wind stress on a water surface. *Quart. J. Roy. Meteor. Soc.* **81**, 639.

Clarke, R. H. and Hess, G. D., 1975: On the relation between surface wind and pressure gradient, especially in lower latitudes. *Bound.-Layer Meteor.* **9**, 325–339.

Claussen, M., 1990: Area-averaging of surface fluxes in a neutrally stratified, horizontally inhomogeneous atmospheric boundary layer. *Atmos. Environ.* **24A**, 1349–1360.

De Rooy, W. C., 1995: Regionalisation of meteorological parameters. *Scientific Report* **WR95-06**. Royal Netherlands Meteorological Institute.

De Rooy, W. C. and Holtslag, A. A. M., 1999: Estimation of surface radiation and energy flux densities from single-level weather data. *J. Appl. Meteor.* **38**, 526–540.

De Wit, A. J. W., Van der Heijden, T. G. C. and Thunnissen, H. A. M., 1999: Vervaardiging en nauwkeurigheid van het LGN3 grondgebruiksbestand. *Report* **663**. DLO-Staring Centrum, Wageningen.

Deaves, D. M., 1981: Computations of wind flow over changes in surface roughness. *J. Wind Eng. Ind. Aerodyn.* **7**, 65–94.

Duijm, N. J., 1983: Model voor de stroming in een neutrale oppervlakte laag na een verandering in oppervlakte ruwheid. in Dutch. *Scientific Report* **WR 83-3**. Royal Netherlands Meteorological Institute.

Elliott, W. P., 1958: The growth of the atmospheric internal boundary layer. *Trans. Amer. Geophys. Union* **29**, 1048–1054.

Frenzen, P. and Vogel, C. A., 1995: On the magnitude and apparent range of variation of the von Karman constant in the atmospheric surface layer. *Bound.-Layer Meteor.* **72**, 371–392. see also *Bound.-Layer Meteor.* **75**, 315–317.

Garratt, J. R., 1977: Review of drag coefficients over oceans and continents. *Mon. Wea. Rev.* **105**, 915–929.

Garratt, J. R., 1990: The internal boundary layer — a review. *Bound.-Layer Meteor.* **50**, 171–203.

Garratt, J. R., 1992: *The Atmospheric Boundary Layer.* Cambridge University Press. Cambridge.

Hess, G. D., 1973: On Rossby-number similarity theory for a baroclinic planetary boundary layer. *J. Atmos. Sci.* **30**, 1722–1723.

Holtslag, A. A. M. and Van Ulden, A. P., 1983: A simple scheme for daytime estimates of the surface fluxes from routine weather data. *J. Clim. Appl. Meteor.* **22**, 517–529.

Horst, T. W., 1999: The footprint for estimation of atmosphere-surface exchange fluxes by profile techniques. *Bound.-Layer Meteor.* **90**, 171–188.

Horst, T. W. and Weil, J. C., 1992: Footprint estimation for scalar flux measurements in the atmospheric surface layer. *Bound.-Layer Meteor.* **59**, 279–29.

Hutjes, R. W. A., 1996: *Transformation of near-surface meteorology in a small-scale landscape with forests and arable land.* PhD thesis. Rijksuniversiteit Groningen, the Netherlands.

Jackson, N. A., 1976: The propagation of modified flow downstream of a change in roughness. *Quart. J. Roy. Meteor. Soc.* **102**, 924–933.

Jackson, P. S. and Hunt, J. C. R., 1975: Turbulent wind flow over a low hill. *Quart. J. Roy. Meteor. Soc.* **101**, 929–955.

Jacobs, A. F. G., 1984: The flow around a thin closed fence. *Bound.-Layer Meteor.* **28**, 317–328.

Jensen, N. O., 1978: Change of surface roughness and the planetary boundary layer. *Quart. J. Roy. Meteor. Soc.* **104**, 351–356.

Kljun, N., Rotach, M. W. and Schmid, H. P., 1999: Allocation of surface sources for elevated trace gas fluxes using "backward trajectory"-simulations. *Preprints, 13th Symp. on Boundary Layers and Turbulence.* Dallas, TX. pp. 187–189. Amer. Meteorol. Soc.

Krishnamurti, T. N. and Bounoua, L., 1996: *An introduction to numerical weather prediction techniques.* CRC Press. Boca Raton, Florida.

Kudryavtsev, V. N. and Makin, V. K., 1996: Transformation of wind in the coastal zone. *Scientific Report* **WR 96-04**. Royal Netherlands Meteorological Institute.

Kudryavtsev, V. N., Makin, V. K., Klein Tank, A. M. G. and Verkaik, J. W., 2000: A model of wind transformation over water–land surfaces. *Scientific Report* **WR-2000-01**. Royal Netherlands Meteorological Institute.

Luthardt, H. and Hasse, L., 1981: On the relationship between surface and geostrophic wind in the region of the German Bight. *Beitr. Phys. Atmosph.* **54**, 222–237.

Mahrt, L., 2000: Surface heterogeneity and vertical structure of the boundary layer. *Bound.-Layer Meteor.* **96**, 33–62.

Marsden, R. F., 1987: A comparison between geostrophic and directly measured surface winds over the Northeast Pacific ocean. *Atmos.-Ocean* **25**, 387–401.

Obukhov, A. M., 1971: Turbulence in an atmosphere with a non-uniform temperature. *Bound.-Layer Meteor.* **2**, 7–29.

Panofsky, H. A. and Dutton, J. A., 1984: *Atmospheric Turbulence, Models and Methods for Engineering Applications.* Jon Wiley & Sons. New York.

Pasquill, F., 1972: Some aspects of boundary layer description. *Quart. J. Roy. Meteor. Soc.* **98**, 469–494.

Rijkoort, P. J., 1983: A compound Weibull model for the description of surface wind velocity distributions. *Scientific Report* **WR 83-13**. Royal Netherlands Meteorological Institute.

Rijkoort, P. J. and Wieringa, J., 1983: Extreme wind speeds by compound Weibull analysis of exposure-corrected data. *J. Wind Eng. Ind. Aerodyn.* **13**, 93–104.

Schmid, H. P., 1994: Source areas for scalars and scalar fluxes. *Bound.-Layer Meteor.* **67**, 293–318.

Shir, C. C., 1972: A numerical computation of air flow over a sudden change of surface roughness. *J. Atmos. Sci.* **29**, 304–310.

Smits, A., 2001a: Analysis of the Rijkoort-Weibull model. *Technical Report* **TR-232**. Royal Netherlands Meteorological Institute.

Smits, A., 2001b: Estimation of extreme return levels of wind speed: an analysis of storm maxima. *Report* **Hydra project**. Royal Netherlands Meteorological Institute.

Taylor, P. A., 1987: Comments and further analysis on effective roughness lengths for use in numerical models. *Bound.-Layer Meteor.* **39**, 403–418.

Tennekes, H., 1973: The logarithmic wind profile. *J. Atmos. Sci.* **30**, 234–238.

Townsend, A. A., 1965: The response of a turbulent boundary layer to abrupt changes in surface conditions. *J. Fluid Mech.* **22**, 799–822.

Troen, I. and Petersen, E. L., 1989: *European Wind Atlas.* Risø National Laboratory. Roskilde, Denmark.

Van Wijk, A. J. M., Beljaars, A. C. M., Holtslag, A. A. M. and Turkenburg, W. C., 1990: Diabatic wind speed profiles in coastal regions: comparison of an internal boundary layer (IBL) model with observations. *Bound.-Layer Meteor.* **51**, 49–74.

Verkaik, J. W., 2000: Evaluation of two gustiness models for exposure correction calculations. *J. Appl. Meteor.* **39**, 1613–1626.

Walmsley, J. L., 1989: Internal boundary-layer height formulae — a comparison with atmospheric data. *Bound.-Layer Meteor.* **47**, 251–262.

Wieringa, J., 1976: An objective exposure correction method for average wind speeds measured at a sheltered location. *Quart. J. Roy. Meteor. Soc.* **102**, 241–253.

Wieringa, J., 1986: Roughness-dependent geographical interpolation of surface wind speed averages. *Quart. J. Roy. Meteor. Soc.* **112**, 867–889.

Wieringa, J. and Rijkoort, P. J., 1983: *Windklimaat van Nederland.* Staatsuitgeverij. Den Haag, the Netherlands.

Appendix A

Tables

Table A.1: Land use classes in LGN3+ and the assigned roughness lengths.

ID	Class Name	z_0 (m)
0	no data	0.03
1	grass	0.03
2	maize	0.17
3	potatoes	0.07
4	beets	0.1
5	cereals	0.16
6	other agricultural crops	0.04
8	greenhouses	0.1
9	orchards	0.39
10	bulb cultivation	0.1
11	deciduous forest	0.75
12	coniferous forest	0.75
16	fresh water	0.001
17	salt water	0.001
18	continuous urban area	1.6
19	built-up in rural area	0.5
20	deciduous forest in urban area	1.1
21	coniferous forest in urban area	1.1
22	built-up area with dense forest	2.
23	grass in built-up area	0.03
24	bare soil in built-up area	0.001
25	main roads and railways	0.1
26	buildings in rural area	0.5
27	runways	0.0003
28	parking lots	0.1
30	salt marshes	0.0002
31	beaches and dunes	0.0003
32	sparsely vegetated dunes	0.06
33	vegetated dunes	0.02
34	heathlands in dune areas	0.03
35	shifting sands	0.0003
36	heathlands	0.03
37	heathlands with minor grass influence	0.04
38	heathlands with major grass influence	0.06
39	raised bogs	0.06
40	forest in raised bogs	0.75
41	miscellaneous swamp vegetation	0.03
42	reed swamp	0.1
43	forest in swamp areas	0.75
44	swampy pastures in peat areas	0.07
45	herbaceous vegetation	0.03
46	bare soil in natural areas	0.001

Table A.2: Numbers and names of the stations used in the validation. At the stations with stars stability information is available.

Number	Name	Number	Name
210	Valkenburg*	290	Twenthe*
225	IJmuiden	308	Cadzand
229	Texelhors	310	Vlissingen*
235	De Kooy*	311	Hoofdplaat
240	Schiphol*	312	Oosterschelde
242	Vlieland	313	Vlakte van de Raan
248	Wijdenes	315	Hansweert
250	Terschelling	316	Schaar
251	Hoorn (Terschelling)	320	Lichteiland Goeree
252	K13	321	Europlatform
254	Meetpost Noordwijk	323	Wilhelminadorp
260	De Bilt*	324	Stavenisse
265	Soesterberg*	330	Hoek van Holland*
269	Lelystad	331	Tholen
270	Leeuwarden*	340	Woensdrecht
271	Stavoren-Haven	343	Rotterdam Geulhaven
273	Marknesse	344	Zestienhoven*
275	Deelen*	348	Cabauw
277	Lauwersoog	350	Gilze-Rijen*
278	Heino	356	Herwijnen
279	Hoogeveen	370	Eindhoven*
280	Eelde*	375	Volkel*
283	Hupsel	377	Ell
285	Huibertgat	380	Beek*
286	Nieuw Beerta	391	Arcen

Appendix B

Figures

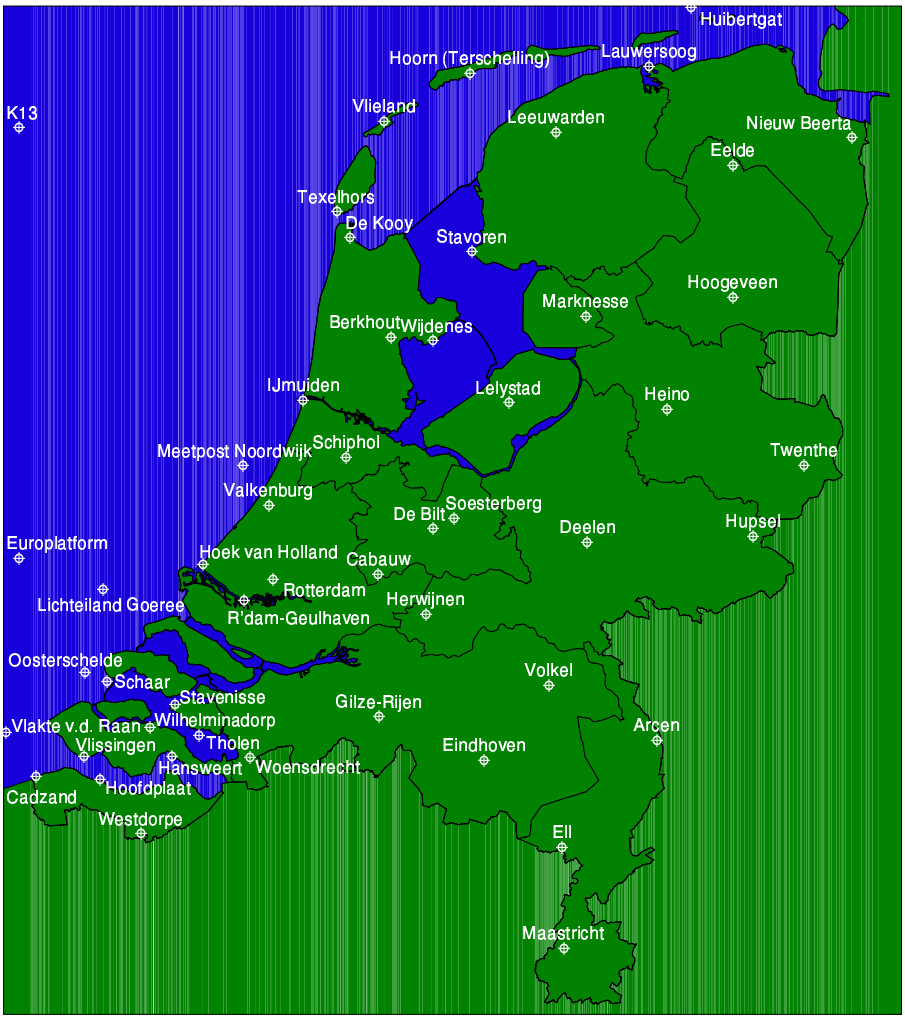

Figure B.1: The wind speed measurement network in the Netherlands.

(a) Roughness map (100 m)^2-pixels, 10 roughness classes. Dark areas are smooth, bright areas are rough. The station is in the middle of the map.

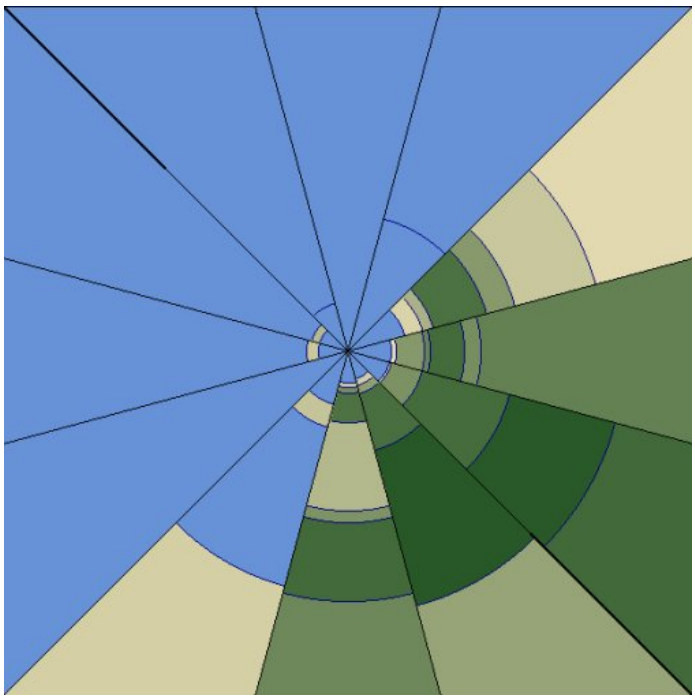

(b) Roughness transition analysis of WASP.

Figure B.2: Roughness map of the environment of Lelystad.

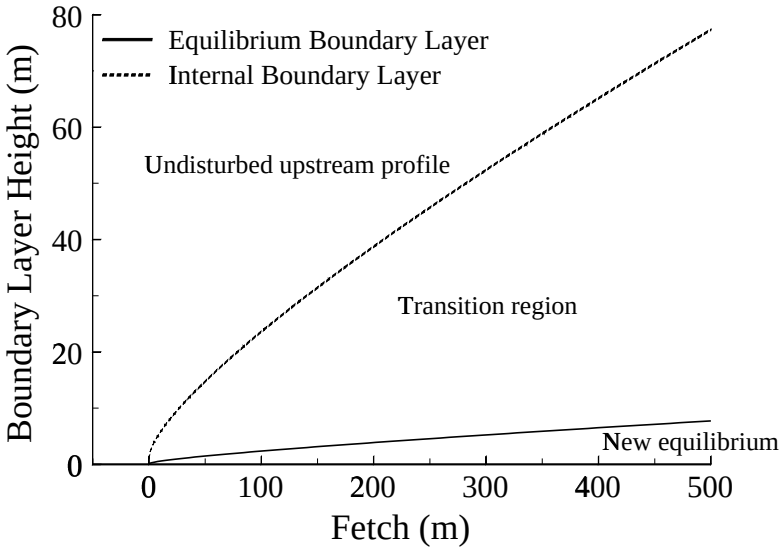

Figure B.3: Development of internal boundary layers after a change in roughness at $x = 0$.

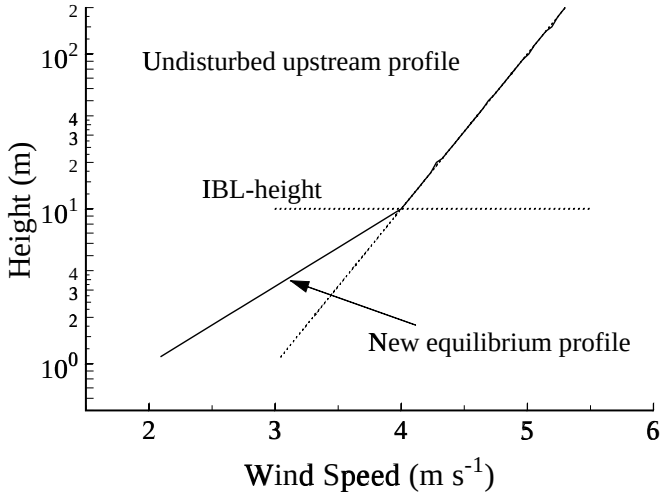

Figure B.4: A simple concept of the wind profile in the IBL.

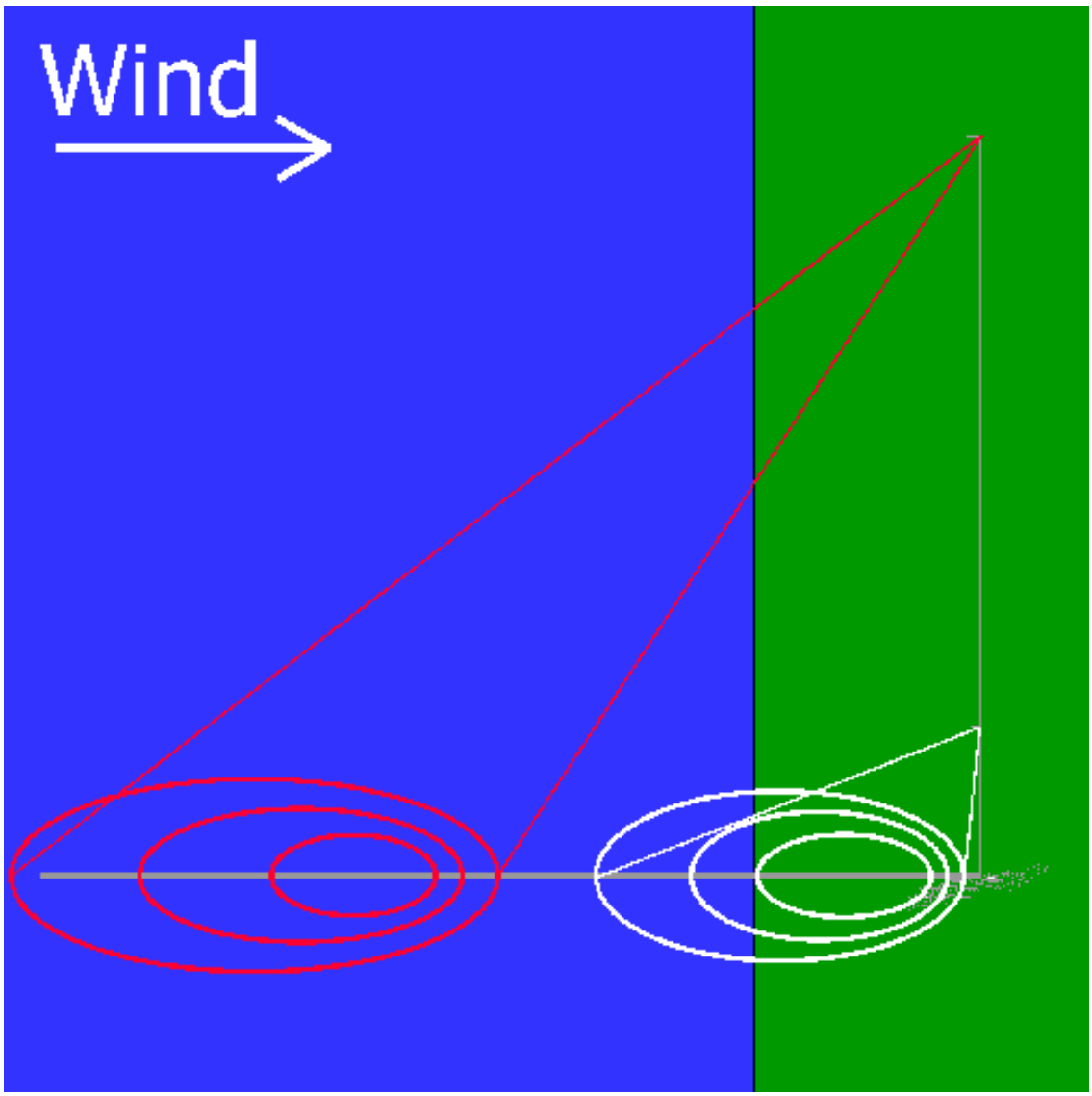

Figure B.5: Illustration of the footprint for two different measuring height nearby a coastline.

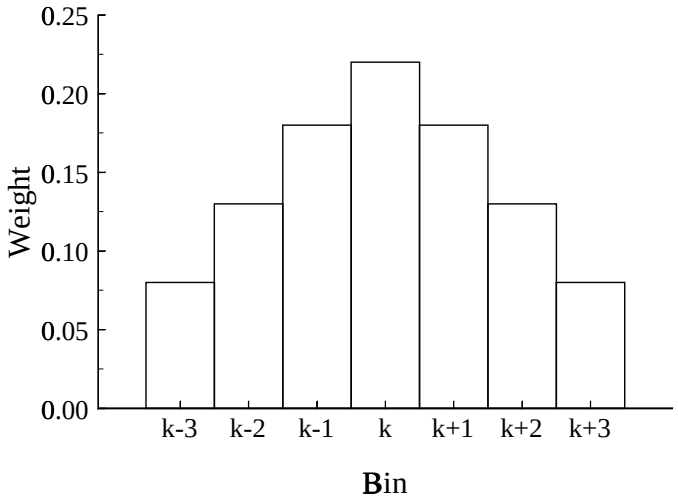

Figure B.6: Smoothing function for the 5° wide wind direction source areas.

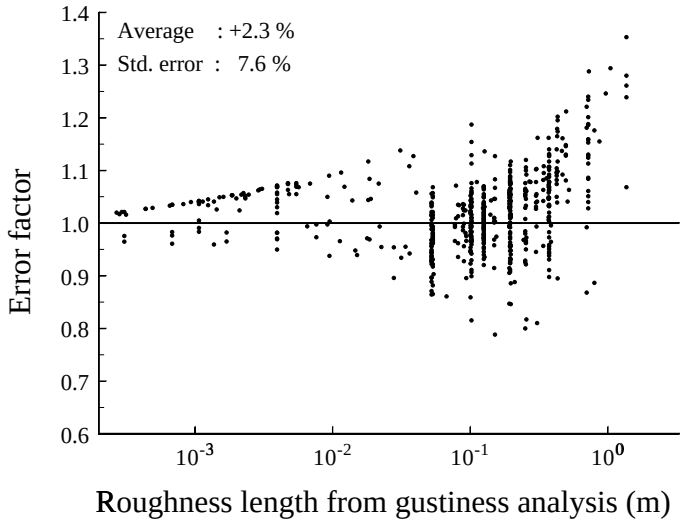

Figure B.7: Comparison of roughness lengths derived from gustiness and land-use. An error factor larger than 1 implies the gustiness roughness is larger than the land-use roughness.

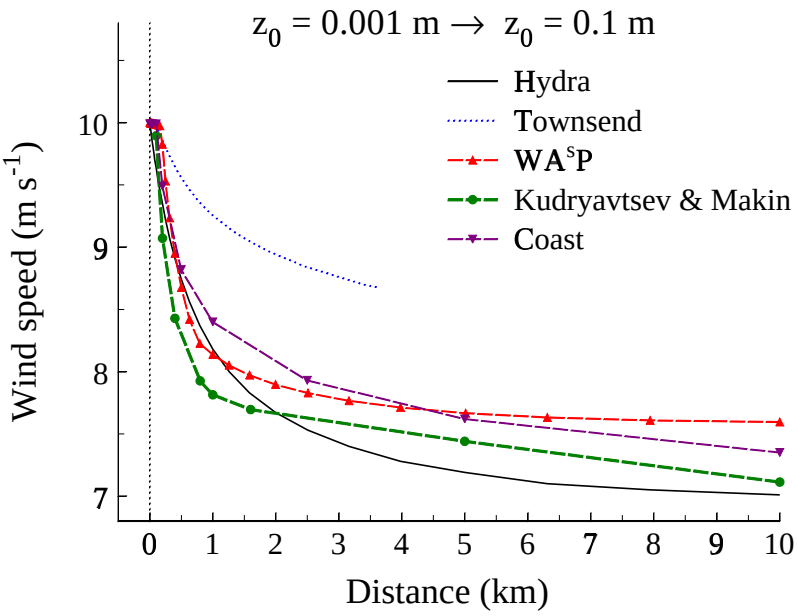

(a) Smooth-to-rough transition

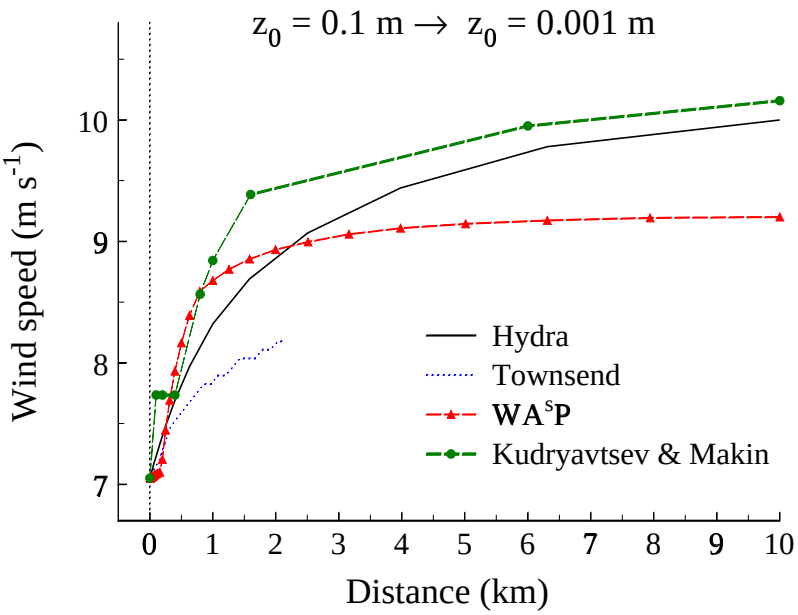

(b) Rough-to-smooth transition

Figure B.8: The development of the wind speed in the two-layer model (Hydra) compared with IBL-models.

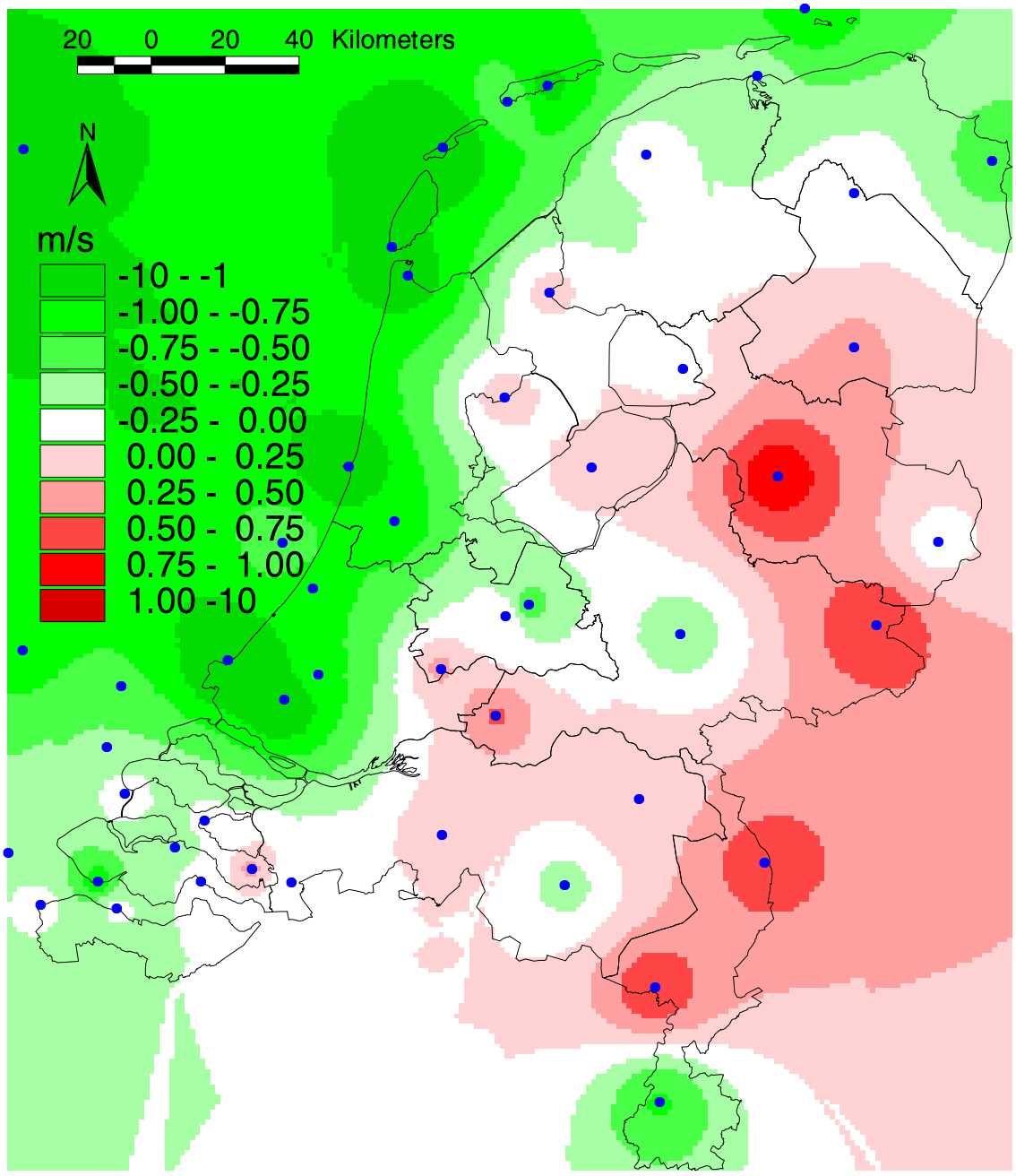

Figure B.9: Bias in average surface wind speed (Estimated−Measured). Uniform macrowind.

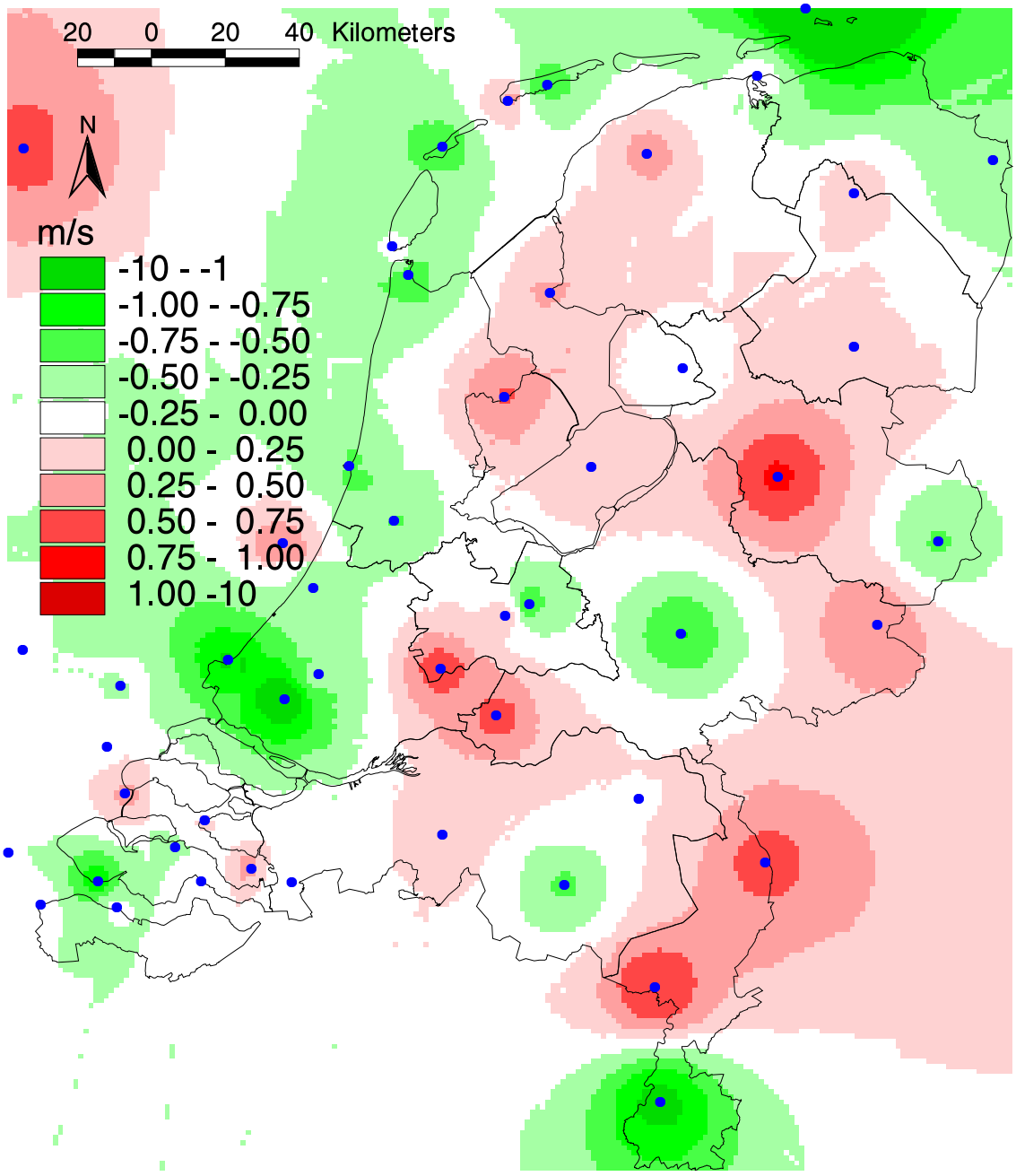

Figure B.10: Bias in average surface wind speed (Estimated−Measured). $R = 140$ km.

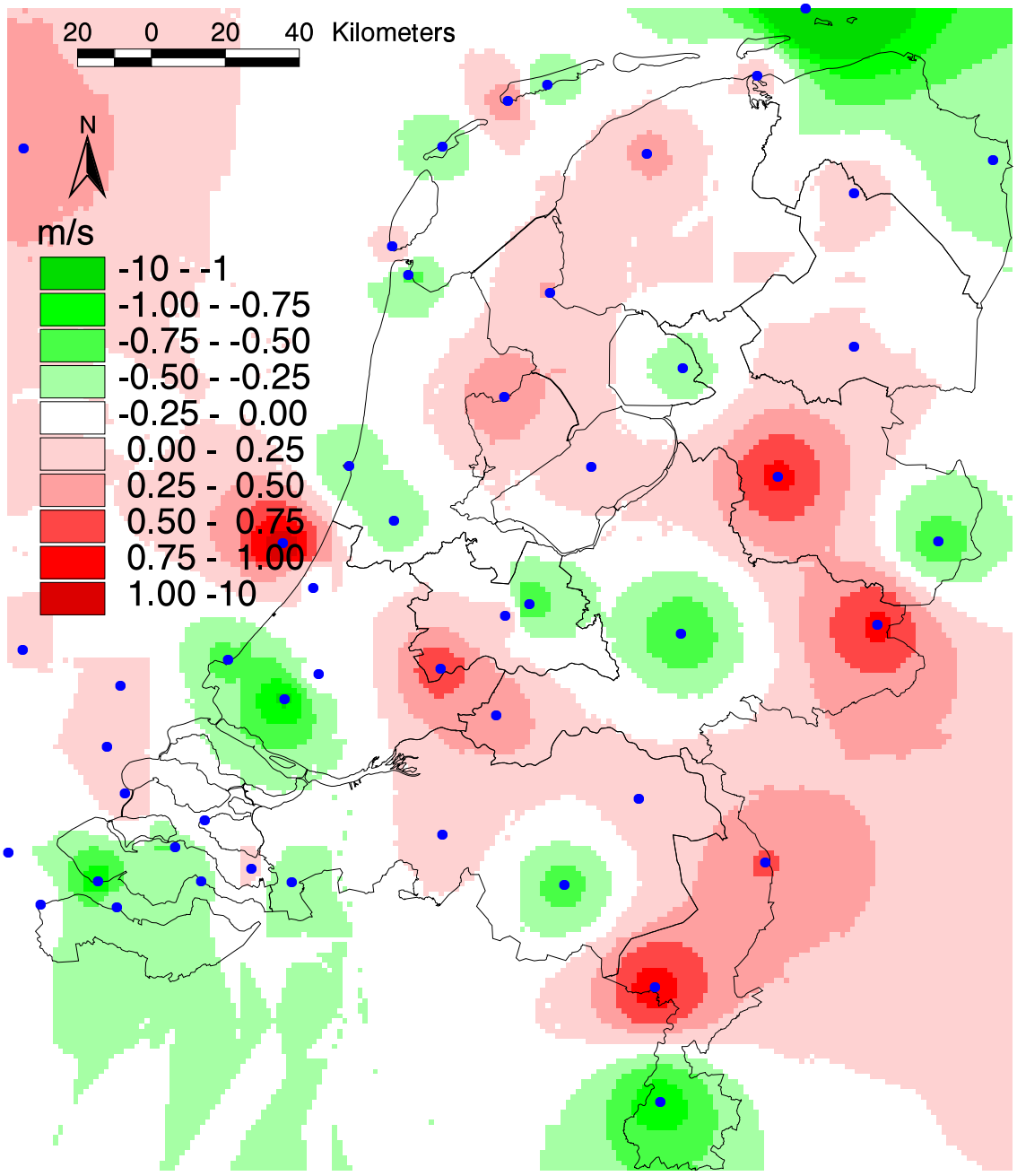

Figure B.11: Bias in average surface wind speed (Estimated−Measured). $R = 70$ km.

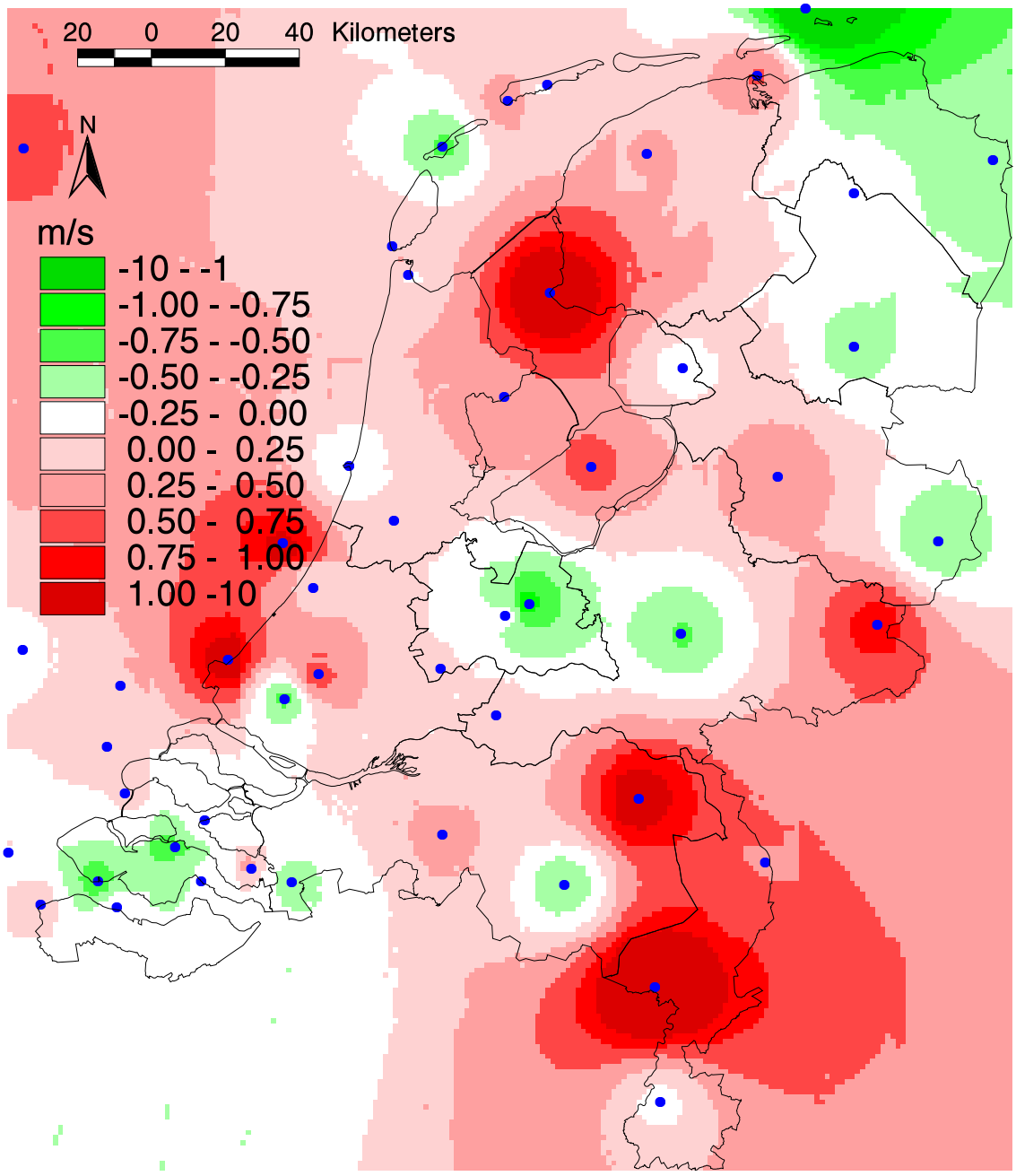

Figure B.12: Bias in average surface wind speed (Estimated−Measured). $R = 20$ km.

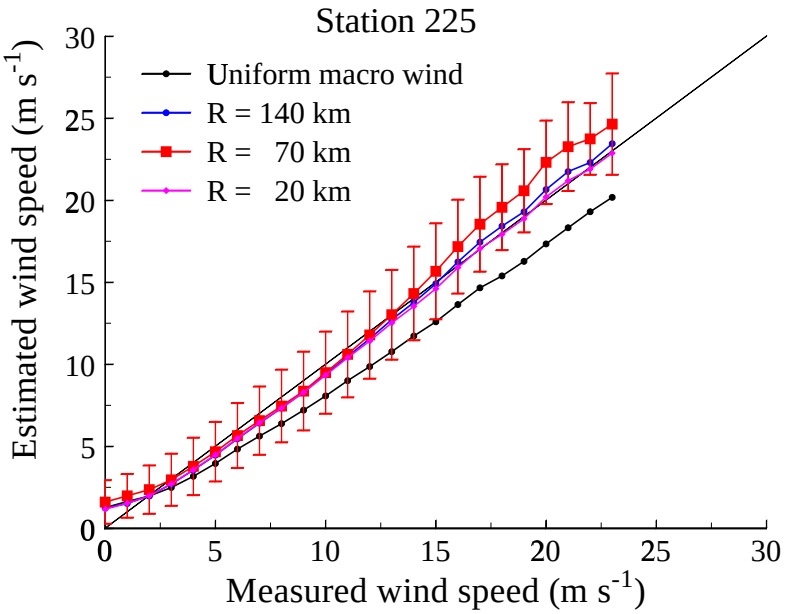

Figure B.13: Wind speed dependence of the simulated wind speed for the four runs at station 225 IJmuiden.

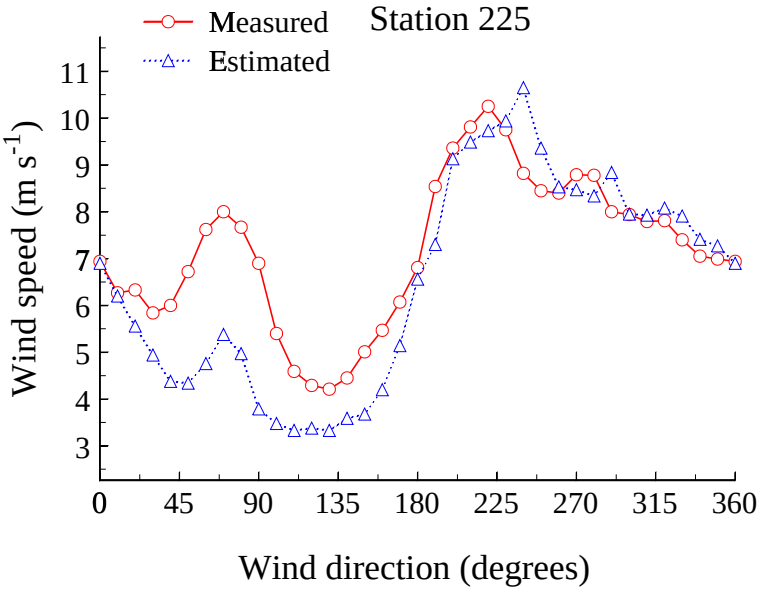

Figure B.14: Average wind speed (measured and simulated) as function of wind direction for $R = 70$ km at station 225 IJmuiden. Data selection $U_{\text{meas}} \geq 2$ m s^{-1}.

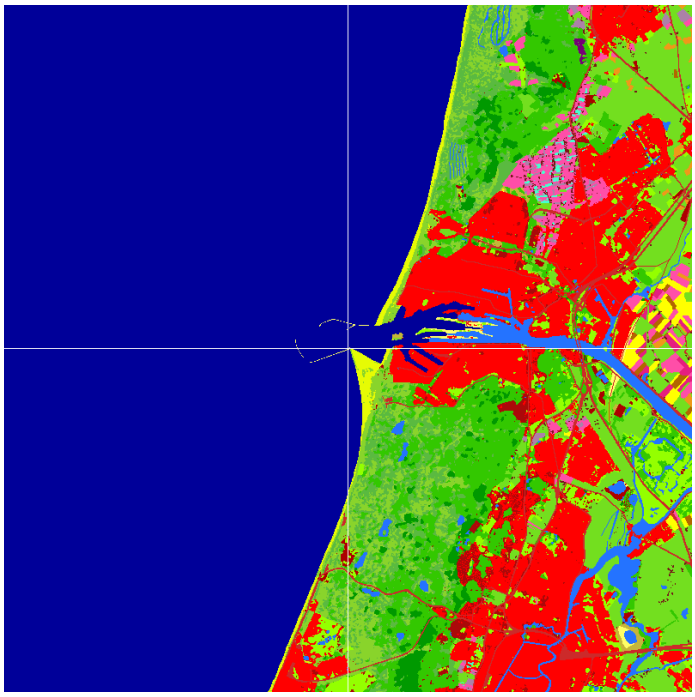

Figure B.15: Land use map of station 225 IJmuiden and it's environment. Area $(20\ \mathrm{km})^2$.

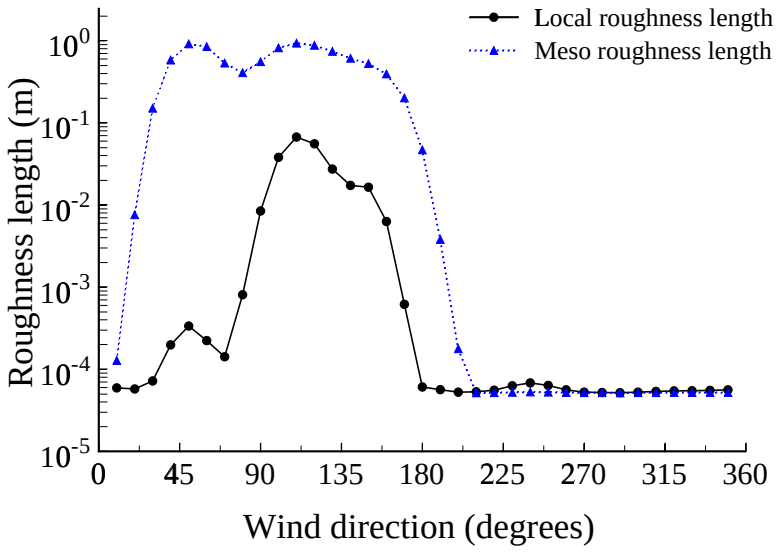

Figure B.16: Land use derived roughness length (meso and local) of station 225 IJmuiden as function of wind direction.

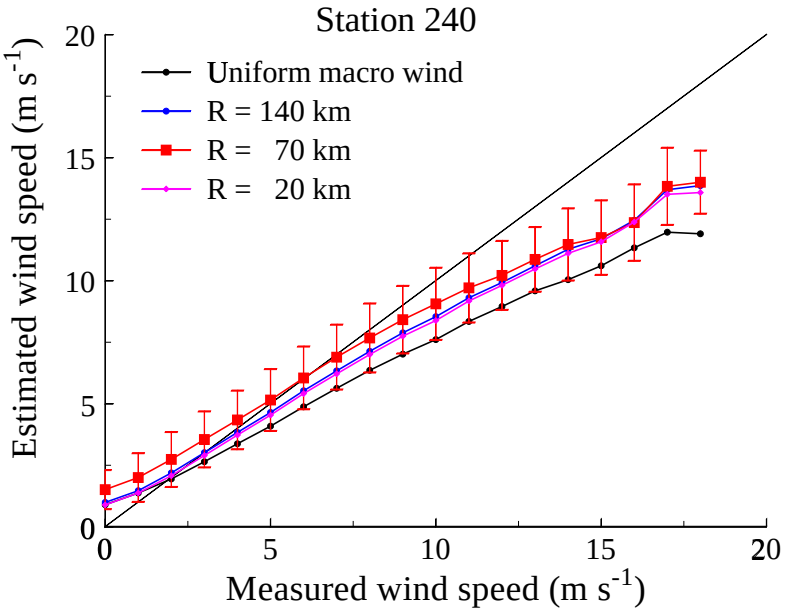

Figure B.17: Wind speed dependence of the simulated wind speed for the four runs at station 240 Schiphol.

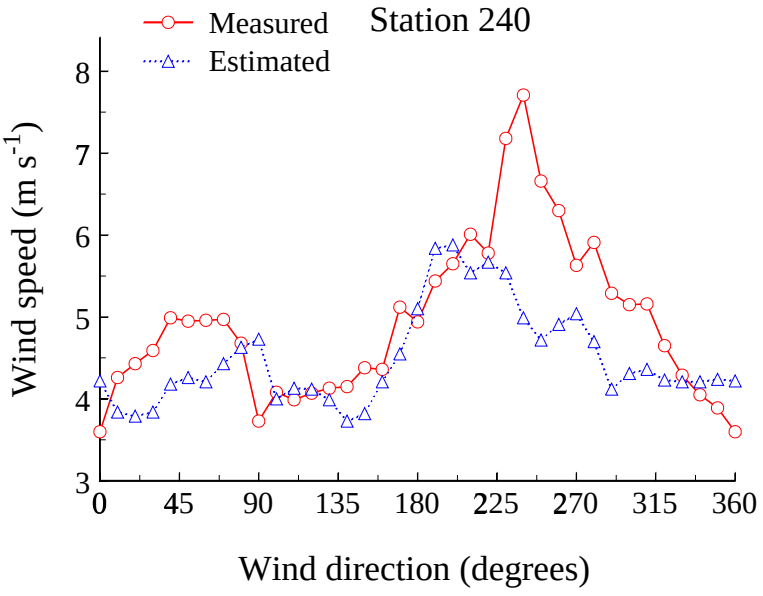

Figure B.18: Average wind speed (measured and simulated) as function of wind direction for $R = 70$ km at station 240 Schiphol. Data selection $U_{\text{meas}} \geq 2$ m s^{-1}.

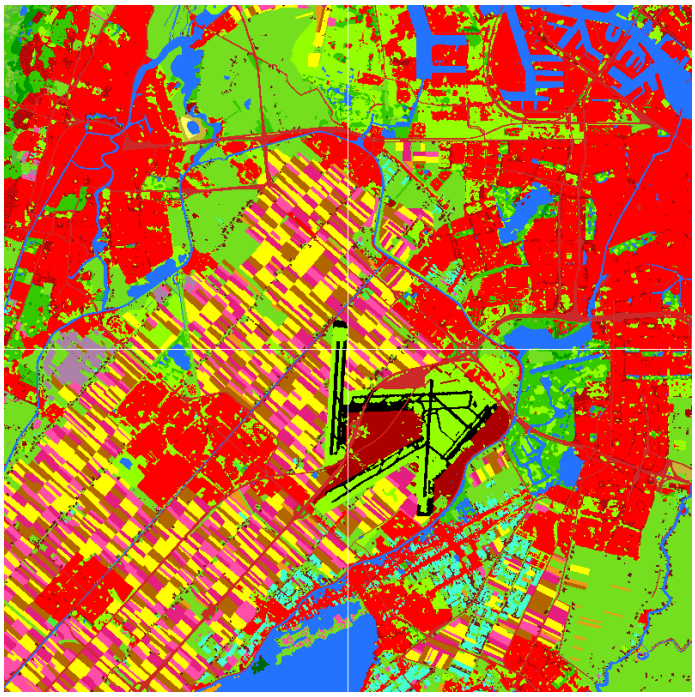

Figure B.19: Land use map of station 240 Schiphol and it's environment. Area $(20\ \mathrm{km})^2$.

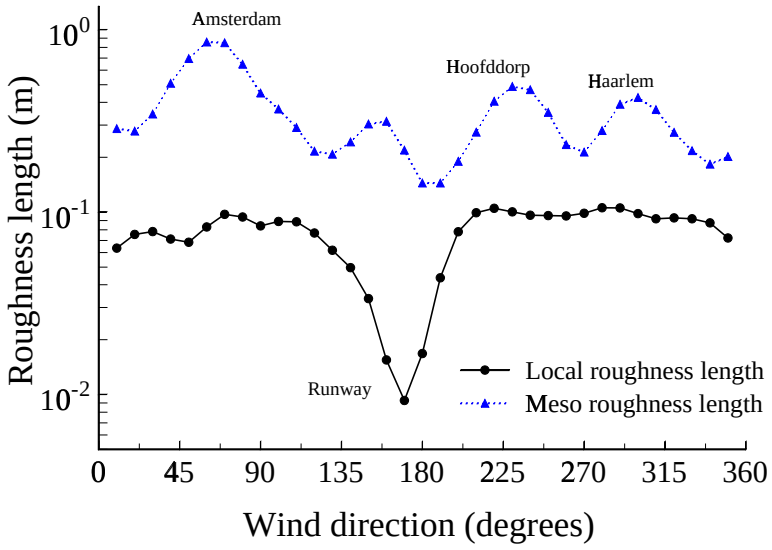

Figure B.20: Land use derived roughness length (meso and local) of station 240 Schiphol as function of wind direction.

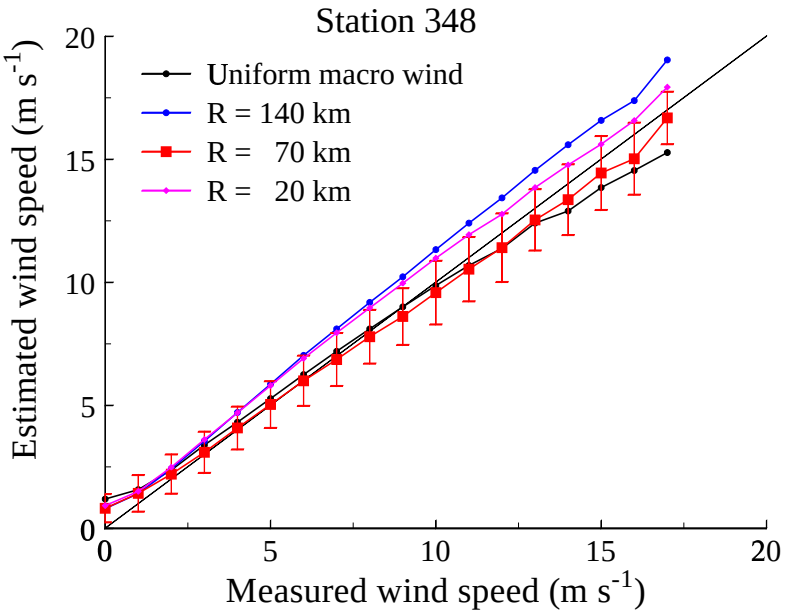

Figure B.21: Wind speed dependence of the simulated wind speed for the four runs at station 348 Cabauw.

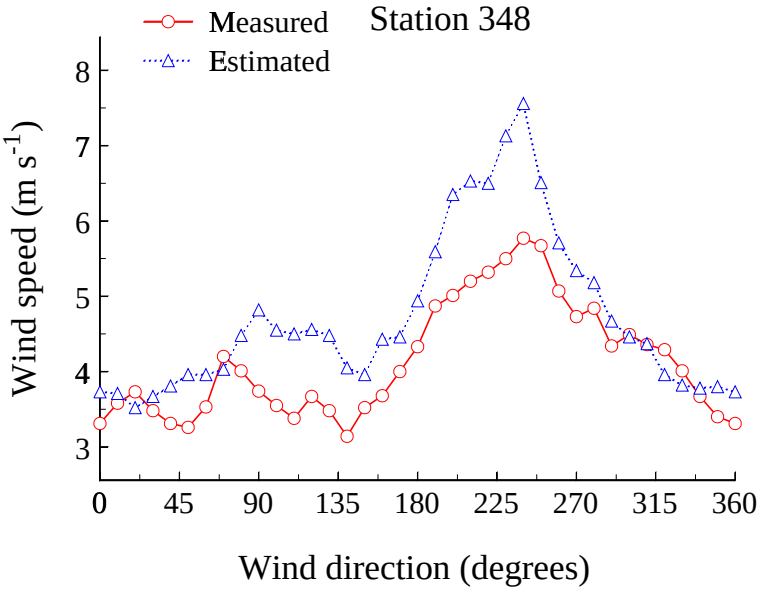

Figure B.22: Average wind speed (measured and simulated) as function of wind direction for $R = 70$ km at station 348 Cabauw. Data selection $U_{\text{meas}} \geq 2$ m s^{-1}.

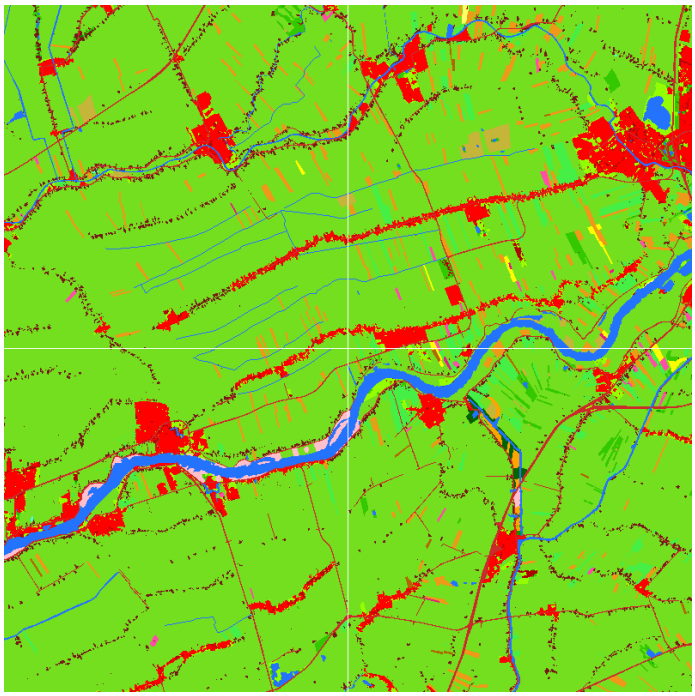

Figure B.23: Land use map of station 348 Cabauw and it's environment. Area $(20\ \mathrm{km})^2$.

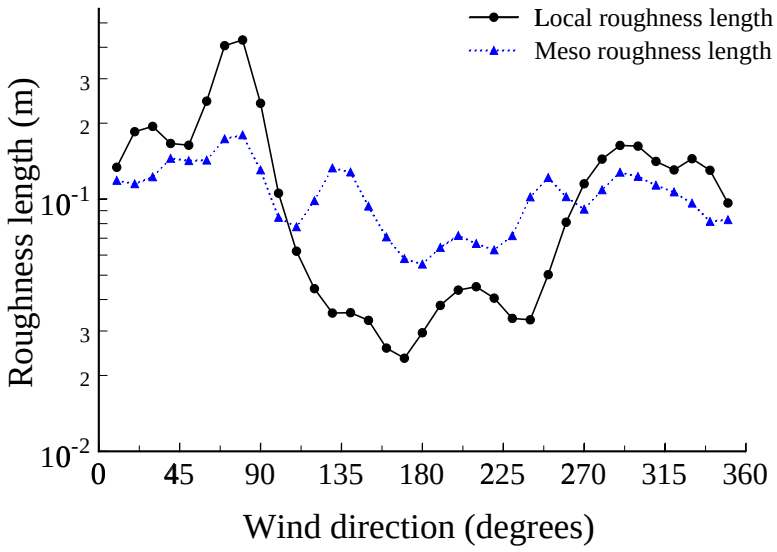

Figure B.24: Land use derived roughness length (meso and local) of station 348 Cabauw as function of wind direction.

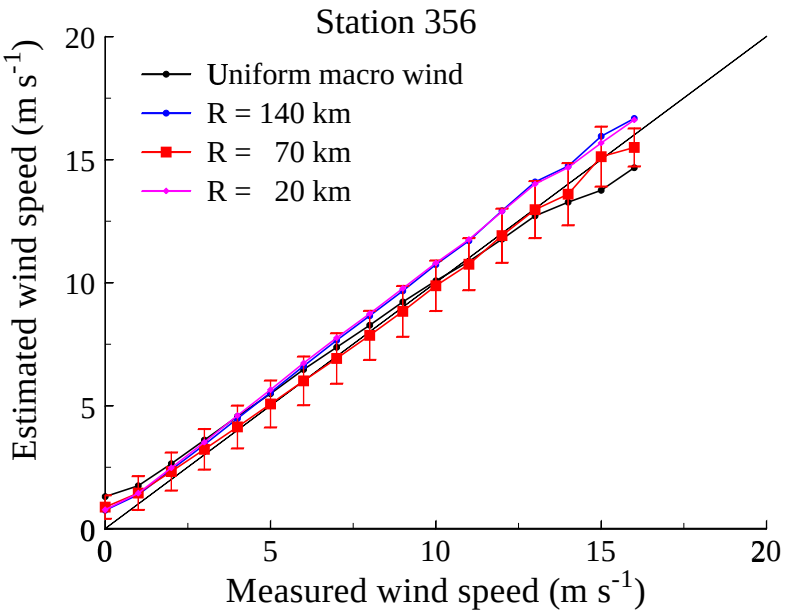

Figure B.25: Wind speed dependence of the simulated wind speed for the four runs at station 356 Herwijnen.

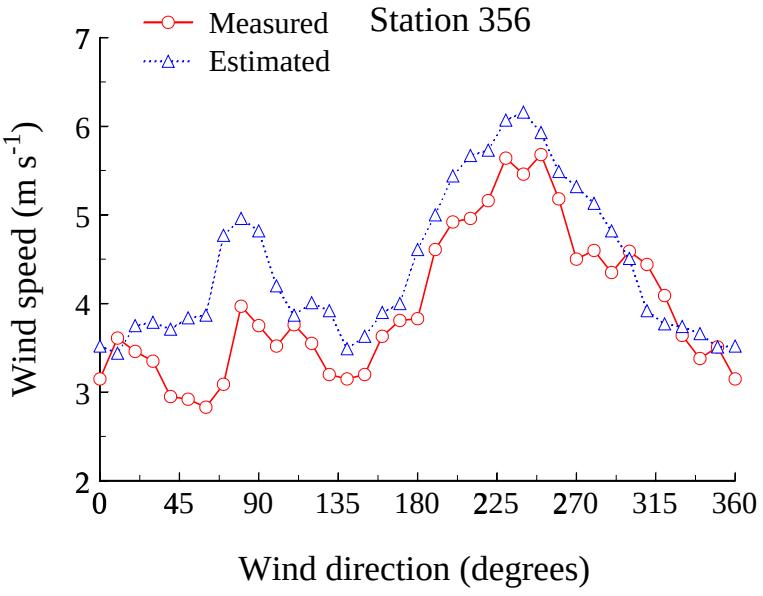

Figure B.26: Average wind speed (measured and simulated) as function of wind direction for $R = 70$ km at station 356 Herwijnen. Data selection $U_{\text{meas}} \geq 2$ m s^{-1}.

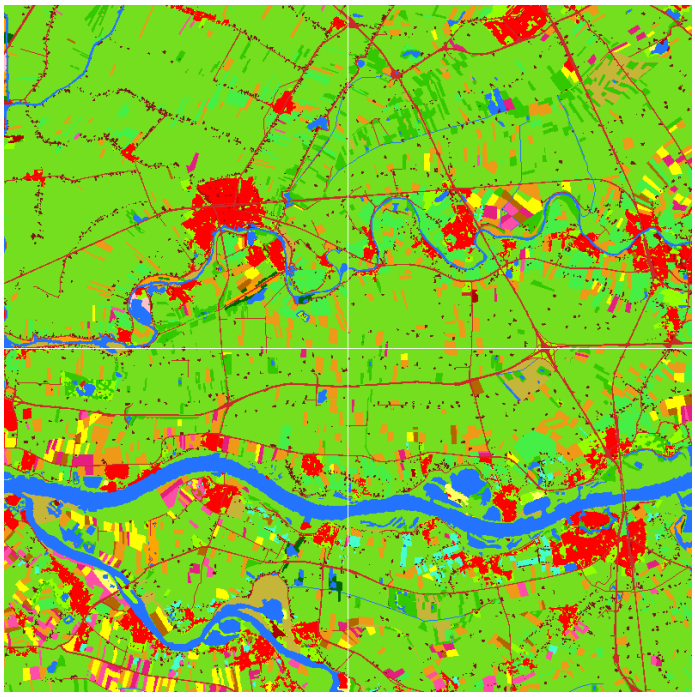

Figure B.27: Land use map of station 356 Herwijnen and it's environment. Area $(20\ \mathrm{km})^2$.

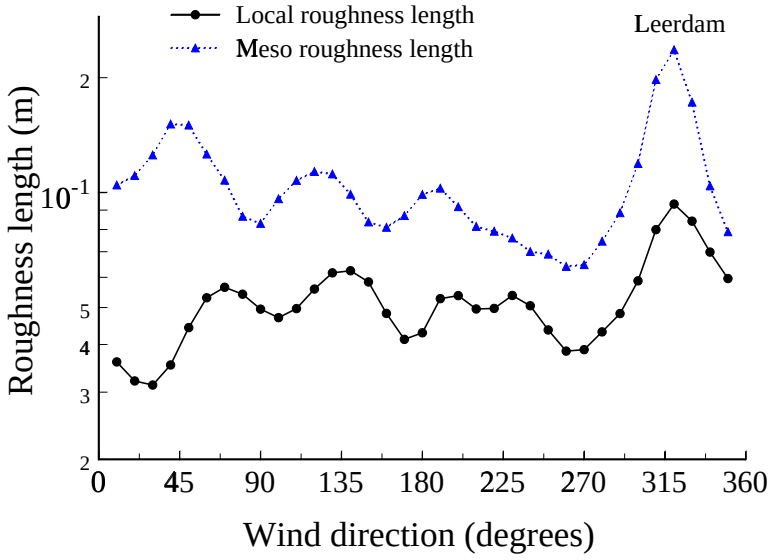

Figure B.28: Land use derived roughness length (meso and local) of station 356 Herwijnen as function of wind direction.

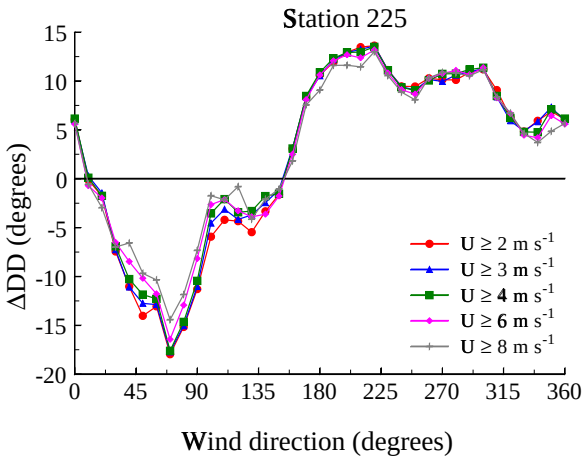

(a) Bias in wind direction.

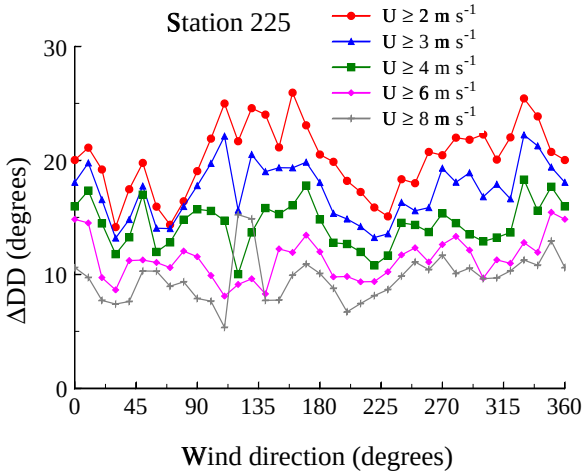

(b) Standard deviation of the wind direction error.

Figure B.29: Bias and standard deviation of the wind direction error for station 225 IJmuiden (Estimated−Measured) as function of measured wind direction for different wind speed thresholds.

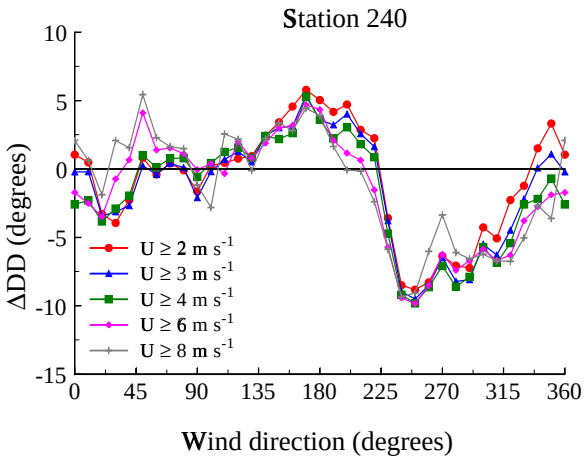

(a) Bias in wind direction.

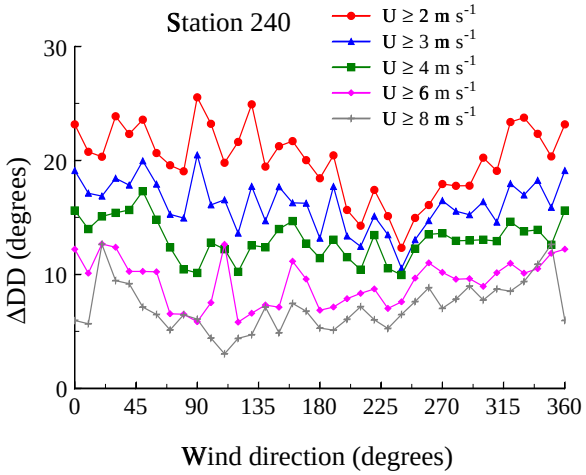

(b) Standard deviation of the wind direction error.

Figure B.30: Bias and standard deviation of the wind direction error for station 240 Schiphol (Estimated−Measured) as function of measured wind direction for different wind speed thresholds.

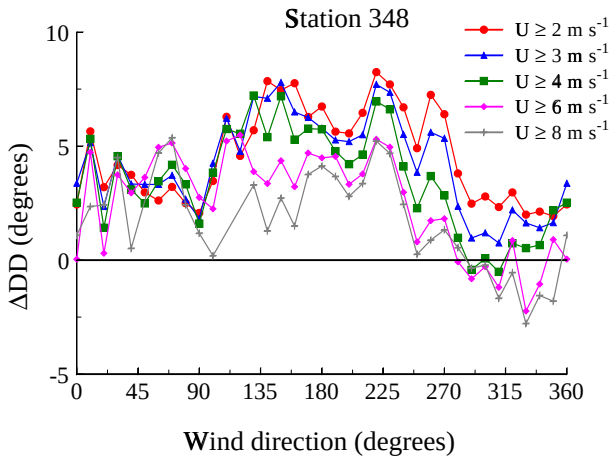

(a) Bias in wind direction.

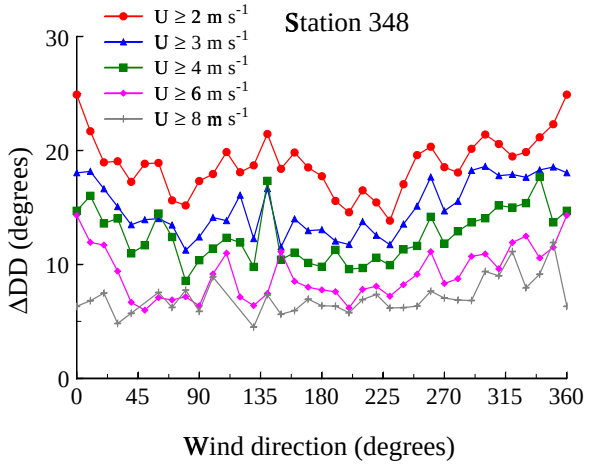

(b) Standard deviation of the wind direction error.

Figure B.31: Bias and standard deviation of the wind direction error for station 348 Cabauw (Estimated−Measured) as function of measured wind direction for different wind speed thresholds.

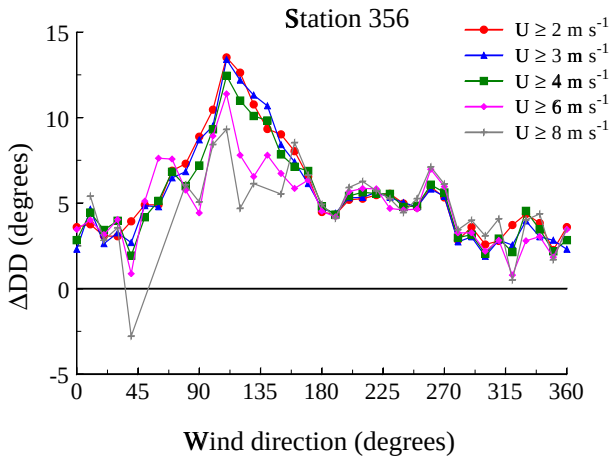

(a) Bias in wind direction.

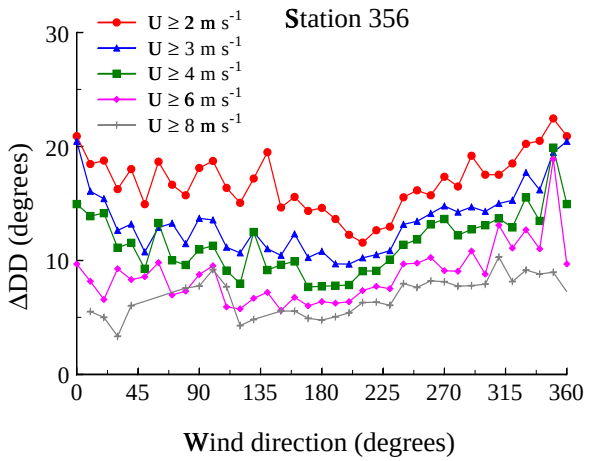

(b) Standard deviation of the wind direction error.

Figure B.32: Bias and standard deviation of the wind direction error for station 356 Herwijnen (Estimated−Measured) as function of measured wind direction for different wind speed thresholds.

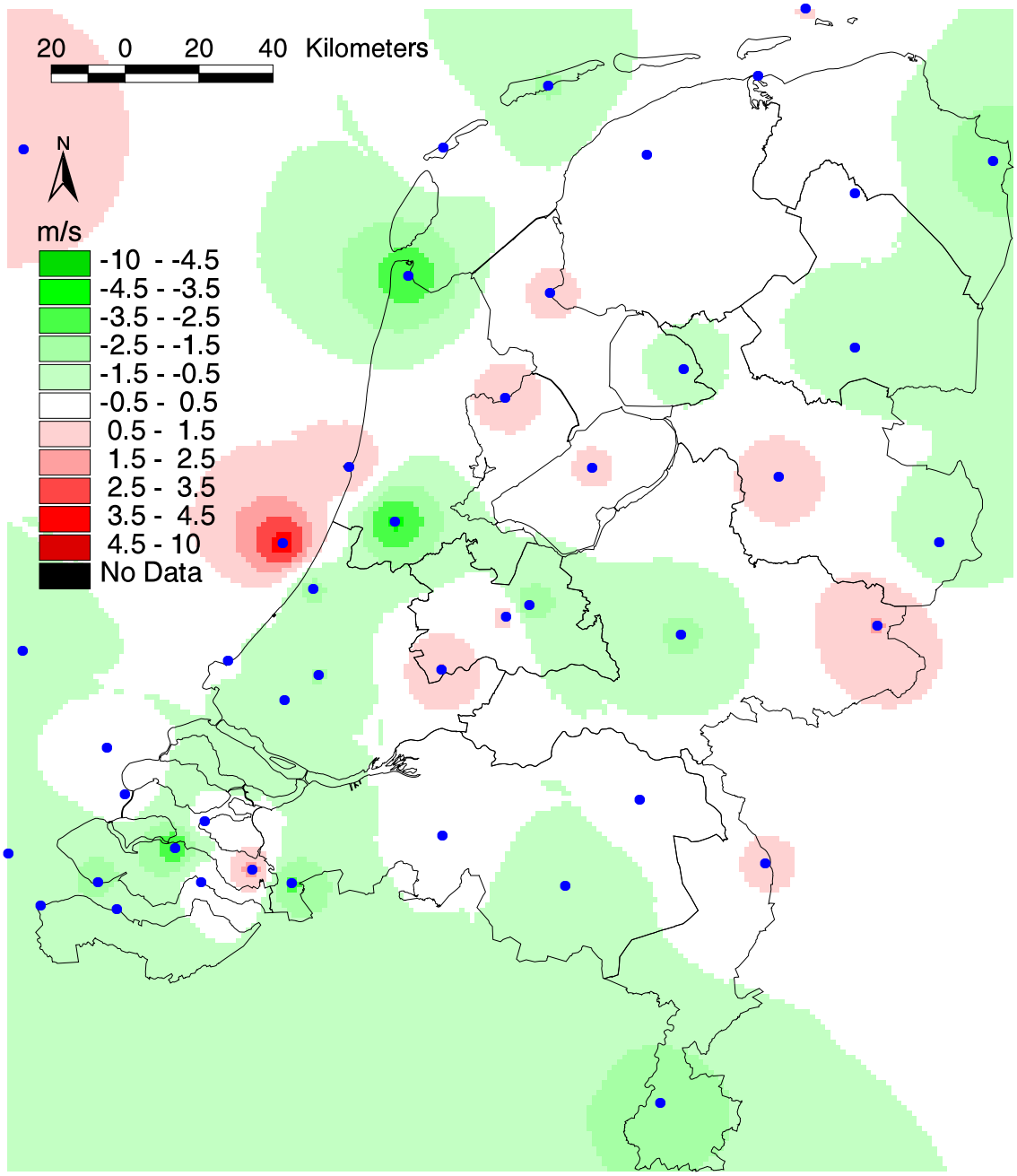

Figure B.33: Bias in potential wind speed (Estimated−Measured) with return period 1 year, season January–February for run 2 ($R = 70$ km).

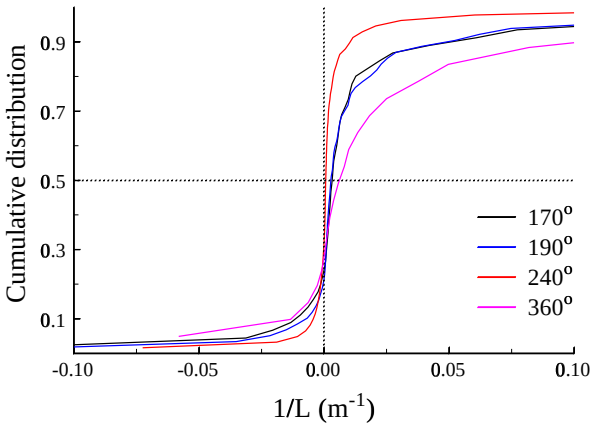

Figure B.34: Cumulative distribution (fraction of total amount) of stability parameter $1/L$, where L is the Obukhov length. Station 240 Schiphol, period 1996–2000, four wind direction sectors.

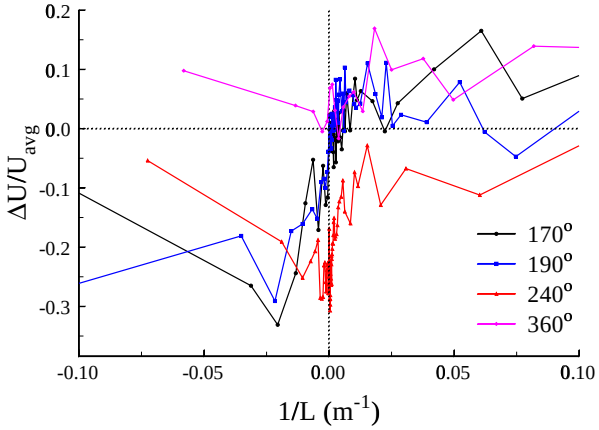

Figure B.35: Stability dependence of relative error in wind speed. One point comprises the average of 30 measurements. Station 240 Schiphol, period 1996–2000, four wind direction sectors.